On The Phase Diagram of the Heisenberg Gamma Model

Sébastien Avakian

A Thesis Submitted to the School of Graduate Studies in
Partial Fulfilment of the Requirements for the Degree Master of Science

August 31, 2023

McMaster University
Master of Science (2023)
Hamilton, Ontario (Department of Physics and Astronomy)

TITLE: On The Phase Diagram of the Heisenberg Gamma Model
AUTHOR: Sébastien Avakian
SUPERVISOR: Dr. Erik S. Sørensen
NUMBER OF PAGES: 66

Acknowledgements

Throughout these last two years, I received a lot of support from various people within my academic circle and outside of it. Firstly, I have to thank my supervisor Erik who provided me with tons of guidance, but also allowed me to make mistakes and develop my own interests within the field. Working with you has made me passionate about numerical techniques and has helped me develop skills I did not know would serve me so well in the future. Thank you for putting up with my near infinite amount of questions that sometimes were as simple as reading input from a file. A big thank you is due to the research group, James, Jonathon, and Addison, you all made my time at McMaster incredibly enjoyable. You were all incredibly welcoming and willing to discuss about seemingly anything, from physics related questions to politics and everything else in between. I also want to thank the physics department as a whole, whether it was during a TAship, lectures, or short chats with someone in the hallway, everyone was kind which has left a special impression on me.

Outside of the academic world, I must deeply thank my partner, Rebecca, who without her support this work would not have been possible. From dealing with my non-stop talk about physics to your support during the long days of work, your presence in my life gives me all the strength I need to press on. Lastly, to my dogs, Faerghus and Mustang, thank you for keeping me company at every moment where you possibly could. You both remind me that there are more important things than work, and that sometimes a smile can go a long way.

Contents

Chapter 1

Introduction

Over the last several decades, quantum spin systems have been a playground for various topics in physics. Whether they emerge from interactions between electrons in the Hubbard model or model magnetic properties in materials, spin systems can provide very exciting physics. Magnetic phenomena has a long and storied history in condensed matter and continues to do so to this day. Spin interactions play important roles in other systems like superconductivity, where electrons of opposite spin can pair up to form a bound state called a cooper pair. Moreover, spin-orbit coupling was also used to propose a topological insulator, a field which has since received massive attention. With topological phenomena in physics attracting a lot of interest due to its potential application to quantum computing, it is natural to wonder what kind of materials we could use to build such a device. It was proposed by Kitaev, that a spin system, called the Honeycomb model, could host a phase that can be used for quantum computation due to its topological nature. This kind of phase has since been named a *quantum spin liquid* as the spins within the system show no long range order and show large entanglement. Since then, several attempts have been made to realize this phase in materials.

Theoretical studies try to discover what the necessary interactions are to host the spin liquid phase and how they effect its stability. This is typically done numerically as spin systems are quite difficult to deal with analytically, where the goal is study the phases admitted by the models. Of the possible set of interactions hypothesised to be important in materials that can host spin liquids, one particular interaction called the Gamma interaction is not well understood. The goal of this work is to understand the role the gamma interaction plays in these systems. In particular, we want to study the Heisenberg and Gamma interaction on a ladder of sites and determine the phases

of this model with the help of the density matrix renormalization group (DMRG), a numerical technique.

The structure of the thesis is as follows: In chapter 2 we present the necessary theoretical background relating to 1D spin chains, numerical techniques and symmetry protected topological phases. Then in chapter 3 the Kitaev honeycomb model is introduced and the origin of the Kitaev spin liquid is explained. Candidate materials are discussed, relevant spin models are presented and the Heisenberg Gama ladder is introduced. In chapter 4 we present the results of the analysis on the Heisenberg Gamma ladder and discuss the phase diagram. We then conclude the work in chapter 5 and have a brief outlook on other research avenues.

Chapter 2

Theory

In this section we introduce the theoretical background related to spin chains relevant to the study of the Heisenberg Gamma ladder. We begin by introducing Lieb-Mathis-Shultz type theorems that allow information of the ground state to be obtained if there exists an energy gap in the system. By using the singular value decomposition's, we derive the Schmidt decomposition of an arbitrary state and use it to probe the bipartite entanglement of the system. Then, by using the area law exhibited by gapped ground states of local Hamiltonians, we show that bounded entanglement entropy in one dimension allows for an approximation of the ground state by the Schmidt decomposition. Matrix product states are then introduced, along with their calculus, with a brief explanation about why they are an efficient representation of 1D spin states. A variational technique known as the density matrix renormalization group is introduced algorithmically and related to the process of renormalization and iterative growth in the finite and infinite context. Lastly, symmetry protected topological states are discussed as the appearance of projective symmetries acting on the matrix product state representation of the 1D spin state.

2.1 1D Spin Chains and Entanglement

2.1.1 Spin Chains And Their Large Hilbert Spaces

One dimensional spin chains are examples of prototypical quantum systems. At low temperatures, such systems provide models for magnetism mediated by the most quintessential quantum property, spin. Examples of such systems are the transverse ising model and its closely related, more general, model the Heisenberg (anti)ferromagnet. Spin

chain systems in general are comprised of many individual spins, and their interactions can severely hinder attempts to study them. We typically represent the spin many body state as a combination as

$$|\psi\rangle = \sum_{\sigma_1,\sigma_2,...,\sigma_N} c_{\sigma_1,\sigma_2,...,\sigma_N}|\sigma_1,\sigma_2,...,\sigma_N\rangle. \tag{2.1}$$

where σ_i is the spin at site i and $|\sigma_1,\sigma_2,...,\sigma_N\rangle = |\sigma_1\rangle\otimes|\sigma_2\rangle...\otimes|\sigma_N\rangle$, i.e. the general spin state is some linear combination of states made from products of single particle states. This means that for N spins, we have a Hilbert space of size 2^N which very quickly becomes problematic when performing calculations analytically or numerically. The former fails to be useful in general as the tools available to probe such systems typically fail in the presence of strong interactions and the latter is typically limited to studying smaller systems sizes ($N \approx 10 - 20$). It is possible to still access the spectrum of such systems through an appropriate unitary transformation by exploiting symmetries and when the interactions are fairly weak, either by perturbation theory or through some sparse numerical solvers. However, this does limit the kinds of systems one can analyze as strongly correlated systems present non zero off diagonal interactions which cannot be ignored and increase the computational complexity of numerical techniques.

Fortunately, condensed matter systems of interest typically involve the first few lowest energy eigenstates, making their analysis tractable. This normally means that the analysis can be restricted to a single state (or set of states) who's nature can be inferred via the symmetries present and some approximation scheme. Some examples include BCS theory [1] and Band Theory both of which have had major success in describing superconductors and low dimensional fermionic systems, respectively, in the thermodynamic limit.

2.1.2 The Heisenberg Antiferromagnetic and the Lieb-Schultz-Mattis Type Theorems

In the case of spin systems, there exists theorems on classes of models that make claims on the nature of the ground state and its energy gap. For example, take the 1D quantum antiferromagnetic Heisenberg Model with periodic boundary conditions:

$$H = J\sum_{i=1}^{L} \mathbf{S_i}\cdot\mathbf{S_{i+1}} + J\mathbf{S_L}\cdot\mathbf{S_1}.$$

where $\mathbf{S} = (S_x, S_y, S_z)$, L is the number of sites in the chain and $J > 0$. If the spins on the chain are of half integer spin, i.e. $S = 1/2, 3/2...$ for L even, then there is

an excitation with energy E_1 such that $E_1 = E_0$ as $L \to \infty$ [2]. In other words, the ground state is degenerate in the thermodynamic limit or said to be gapless. This is primarily due to the fact that half integer spins differ from their original wavefunction when rotated by 2π by a factor of -1. Therefore, due to the SU(2) invariance of the Hamiltonian, one can slightly rotate all of the spins in the x-y plane with

$$U = \exp\left(i\frac{2\pi}{L}\sum_{j=1}^{L} jS_j^z\right).$$

However in 1983 Haldane conjectured that if the spins in the chain have spin 1 the system has a gapped unique ground state which is disordered [3]. Such a contrast in the behaviour of integer vs half integer is surprising and shows that there is an important difference in the behaviour of the ground state based on the kinds of spins in the chain. In general, it is not a trivial task to obtain the ground state of the quantum antiferromagnetic Heisenberg model, but such theorems do offer a place to begin searching for an approximate state that one can begin to analyze in similar spin systems.

2.1.3 The Schmidt Decomposition

One approach in characterizing systems in order to gain information about their low lying states is to study the bipartite entanglement. It is of interest to first rewrite the many body state into a more useful form that naturally allows for the bi-partitioning of the entire system. A pure state $|\psi\rangle$ that is separable by some partition into two subsystems A and B, can be written as

$$|\psi\rangle = \sum_{i,j} C_{ij}|a_i\rangle|b_j\rangle.$$

where $|a_i\rangle \in \mathcal{H}_\mathcal{A}$ and $|b_i\rangle \in \mathcal{H}_\mathcal{B}$ are both bases of their Hilbert spaces of dimension d_A and d_B respectively. If we treat C_{ij} as the entries of a matrix, of dimension $d_A \times d_B$ we can apply the singular value decomposition (SVD) so that $C = USV^\dagger$. The matrices U and $V^\dagger$ are such that

$$U^\dagger U = I, V^\dagger V = I.$$

U and $V^\dagger$ are semi-unitary matrices, the hermitian conjugate of the above equations do not in general equal the identity. As this decomposition holds for any $n \times m$ matrix, the dimensions of these matrices may not in general be the same. The last matrix S is

a diagonal matrix with non-negative entries, $S_{ii} = s_i$, called the singular values and are typically ordered in a decreasing fashion. Using the SVD, we can rewrite our state as

$$|\psi\rangle = \sum_{i,j} \sum_{k=1}^{d} U_{ik} S_{kk} V^*_{jk} |a_i\rangle |b_j\rangle.$$

where $d = \min(d_A, d_B)$ is the smaller of the dimensions of the original matrix. Expanding $\sum_{ij}$ as $\sum_i \sum_j$, we have

$$|\psi\rangle = \sum_{k=1}^{d} s_k \left(\sum_i U_{ik} |a_i\rangle \right) \left(\sum_j V^*_{jk} |b_j\rangle \right) = \sum_{k=1}^{d} s_k |k_A\rangle |k_B\rangle. \tag{2.2}$$

By the properties of U and $V^\dagger$, the bases $\{|k_A\rangle\}$ and $\{|k_B\rangle\}$ are orthonormal bases of $\mathcal{H}_\mathcal{A}$ and $\mathcal{H}_\mathcal{B}$. Finally, restricting the sum to some $r < d$ so that only the non-zero values are included yields the Schmidt Decomposition. The number r is referred to as the Schmidt rank of the state and is quick indicator of the nature of the state while the singular values s_i are called the Schmidt values. If $r = 1$ then the system is just a product state while if $r > 1$ the state is a superposition of several states and is entangled. The main benefit of writing the state in this form is the ease in accessing the entanglement of the state. We can form the density matrix

$$\rho = |\psi\rangle\langle\psi| = \sum_{i=1}^{r} \sum_{j=1}^{r} s_i s_j |i_A\rangle |i_B\rangle \langle j_A| \langle j_B|.$$

Tracing out either subsystem, by exploiting the orthonormality of the states on their subsystem, yields the reduced density matrix on the other

$$\rho_A = \mathrm{Tr}_B(\rho) = \sum_{i=1}^{r} s_i^2 |i_A\rangle\langle i_A|.$$

$$\rho_B = \mathrm{Tr}_A(\rho) = \sum_{j=1}^{r} s_j^2 |j_B\rangle\langle j_B|.$$

This means that both operators have the same eigenvalues even though they are supported on different Hilbert spaces. Crucially, we have that the eigenvalues of the reduced density matrices λ_i are related to the Schmidt values s_i by $\lambda_i = s_i^2$. In this work, we will refer to the eigenspectrum $\{\lambda_i\}$ of $\rho_{A/B}$, the Schmidt values $\{s_i^2\}$, and the singular values $\{s_i\}$ interchangeably as they are all related and contain the same information. Due to the probabilistic interpretation of the density matrix eigenvalues, we must then

have that $\sum_{i=1}^{r} s_i^2 = 1$. Therefore, the von Neumann entropy across the subsystems is simply

$$S_{AB} = -\mathrm{Tr}\left(\rho_A \ln(\rho_A)\right) = -\sum_{i=1}^{d_A} \lambda_i \ln(\lambda_i) = -\sum_{i=1}^{r} s_i^2 \ln(s_i^2). \tag{2.3}$$

In the case where $\lambda_1 = 1$ and the remaining eigenvalues are zero, the bipartite entanglement is zero. This makes sense as the whole state is just a product state, essentially independent from one another. On the other hand, as long as the first eigenvalue is not 1, the sum is non zero and the subsystems exhibit some entanglement between each other. This is also seen through the Schmidt decomposition of a state, shown above, with Schmidt rank $r = 1$. Therefore, if the bipartite entanglement can be accessed, whether through analytical or numerical means, information about the structure of the state can be inferred. It is also important to note that the Schmidt decomposition is possible for any kind of partition or geometry of the system. No specific reference has been made to the *spatial* dimension of the system hosting the pure quantum state. The reason for this is due to the SVD being applicable to matrices of any size. Typically the SVD is only done numerically as the states used to form the Schmidt basis may in general be unwieldy.

2.1.4 The Area Law of Entanglement

Fortunately, S_{AB} is a well studied and known quantity that appears in many different contexts. A quantum state on N sites with local Hilbert space dimension d selected at random has entropy $S_{AB} \approx \frac{N}{2}\ln(d) - \frac{1}{2}$ when the partition cuts the system in half [4]. That is, for an arbitrary quantum state, the entanglement is extensive and therefore scales with the system size. For such a state in D physical dimensions, the bipartite entropy should scale with the *volume* of the partitioned region $S_{AB} \propto L^D$, where L is the length of the system. However, it is possible for ground states of quantum systems that have a gap between the ground state and the excited states and who's interactions are purely local, to follow an *area law* [5]

$$S_{AB} \propto L^{D-1}.$$

In other words, S_{AB} scales with the size of the boundary of the system. Importantly, in one dimension, it means that the entropy is bounded from above by a constant for these gapped state [6, 7]. This has been proven rigorously proven in [6], which was improved upon later in [7], and applies to all 1D gapped systems, not just spin systems. In the case of area law states, The physical picture is that these ground states of gapped local

Hamiltonians in 1D can only contain so much entanglement between partitions. That is, if a 1D chain is partitioned in two, only at the point between the two sections of the chain is there entanglement. The upshot here is that now through (2.3) we have a bound on the eigenvalues of $\rho_{A/B}$ and the Schmidt values in (2.2). In many cases, these gapped ground states also have that the first few Schmidt values are significantly larger than the rest which can be discarded in 1D and 2D [8–11]. This allows such states to be approximated by a finite sum of product states up to some desired precision and provides a very accurate approximation to the true ground state. It is possible that the Schmidt values are all close in value and so there might not be an optimal cutoff as in general there is no way to know what spectrum of $\rho_{A/B}$ will look like. A diagram of these two cases is shown in Fig 2.1. Essentially, the quality of the approximation is determined by

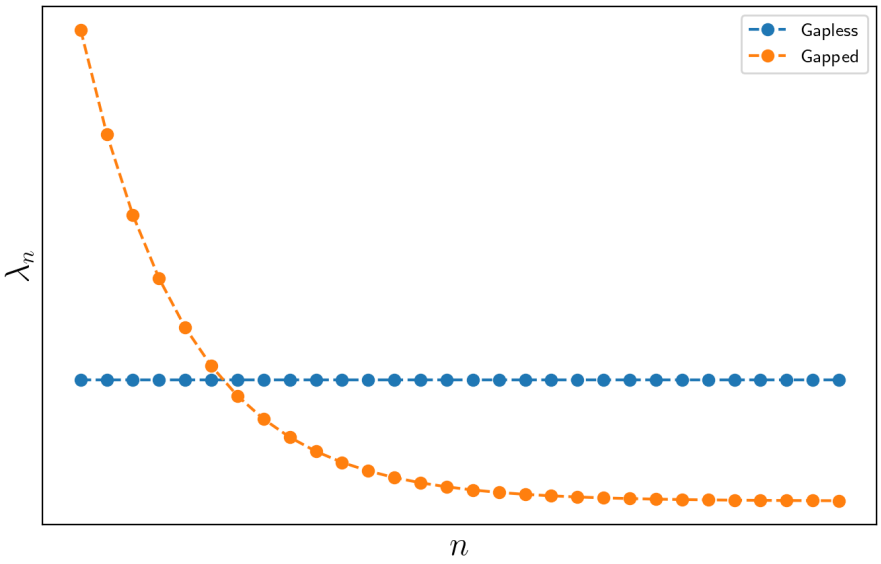

Figure 2.1: Two generic profiles of the spectrum $\{\lambda_n\}$ of the reduced density matrix $\rho_{A/B}$ across a partition. The orange line shows the eigenvalues when the state is gapped while the blue line shows the eigenvalues in the gapped case. For sufficient n, there is an appropriate cutoff n' such the all the λ_k for $k > n'$ can be discarded for the gapped profile. The gapless profile however has no such cutoff.

$$\left|\left||\psi\rangle - \sum_{k=1}^{r'} s_k |k_A\rangle|k_B\rangle\right|\right|. \tag{2.4}$$

where $r' < r$ and r is the Schmidt rank of the state $|\psi\rangle$. That is, if there exists an r' such that (2.4) is bounded above by any delta $\delta > 0$, the state can be well approximated

by the Schmidt Decomposition. For these gapped area law ground states, such an approximation is typically possibly and is intimately related with matrix product state representation of ground states.

2.2 Matrix Product States

2.2.1 From a Many Body State To A Matrix Product State

As mentioned in the previous section, the complete many body state in (2.1) is intractable to deal with in general. Moreover, this general form does not lend itself well to analytical or numerical treatment due the coefficient $c_{\sigma_1,\sigma_2,...,\sigma_N}$ which contains 2^N complex numbers. In general, one can view $c_{\sigma_1,\sigma_2,...,\sigma_N}$ as a *tensor* of rank N in the sense that $c_{\sigma_1,\sigma_2,...,\sigma_N}$ is a multidimensional "matrix". The rank of the tensor is the number of indices it contains, therefore a vector is a rank 1 tensor while a matrix is a rank 2 tensor. When referring to a tensor, its indices are explicitly listed unless there are too many to write down. The indices are said to have a dimension d representing a maximum value that the index can run over. For example, T_{ijk} is the notation of a rank 3 tensor with indices i, j, and k of some arbitrary dimensions while the many body coefficient $c_{\sigma_1,\sigma_2,...,\sigma_N}$ has N indices of dimension $2s+1$ in the case of a spin-s system.

The main use in writing out such indices is that tensors are contracted often in different orders depending on the context. In this work, in order to clarify this order, the sums will be explicitly put in, otherwise the Einstein summation is used: when an index is repeated across more than one tensor, it is implicitly summed over (or contracted). Typically, indices will be primed instead of being outright different to maintain consistency of the notation unless otherwise mentioned.

The main property that will be used to manipulate tensors is the ability to reshape a rank r tensor. Just like a matrix can be reshaped into a vector, a rank r tensor T, can be reshaped into a tensor $\tilde{T}$ of rank $s < r$ as long as the entries of T are appropriately tracked. In other words, there is a bijection between the indices of T and $\tilde{T}$. For example, a rank 3 tensor A_{ijk} can be reshaped into a matrix $M_{ij'}$ where $j' = (j,k) = jk$ is the new index with dimension equal to the product of the dimensions of j and k. When dealing with a wavefunction analytically, whether the many body coefficient in (2.1) is treated as a rank N tensor or a vector of size 2^N is not important, whereas numerically the choice may depend on the task at hand.

Just like a matrix, arbitrary tensors can be decomposed into other smaller rank tensors with an appropriate reshape. Guided by the Schmidt decomposition and the SVD, one can "break" the coefficient of the many body state into N different matrices, similar to what was done to derive equation (2.2). To do this we start with the many body coefficient, treated as a rank N tensor, and isolate the left most index, σ_1 and combine the remaining indices, $\sigma_2, ..., \sigma_N$, as

$$\Psi_{\sigma_1,(\sigma_2,...,\sigma_N)} = \Psi_{\sigma_1,\sigma'} = c_{\sigma_1,\sigma_2,...,\sigma_N}.$$

This reshaped tensor $\Psi_{\sigma_1,\sigma'}$ is a matrix of size $(d \times d^{N-1})$ where $d = 2s + 1$ for spin s. The combined index σ' is a dummy index that we will reuse as a shorthand to group the remaining rightmost indices. We can now use the SVD to write the reshaped tensor as a product

$$\Psi_{\sigma_1,\sigma'} = \sum_{a_1}^{r_1} U_{\sigma_1,a_1} S_{a_1,a_1} V^{\dagger}_{a_1,\sigma'} = \sum_{a_1}^{r_1} U_{\sigma_1,a_1} c_{(a_1,\sigma_2,...,\sigma_N)}.$$

The index that appeared above, a_1, comes from the SVD and will be referred to as a *bond* index of dimension r_1. In the last equality, we multiplied the S_{a_1,a_1} and $V^{\dagger}_{a_1,\sigma'}$ matrices together to recover part of the many body coefficient with a new single index $(a_1, \sigma_2, ..., \sigma_N) = a_1\sigma_2...\sigma_N$. We will rename U_{σ_1,a_1} to $A^{\sigma_1}_{a_1}$ which changes the original tensor to

$$c_{\sigma_1,\sigma_2,...,\sigma_N} = \sum_{a_1}^{r_1} A^{\sigma_1}_{a_1} c_{(a_1,\sigma_2,...,\sigma_N)}.$$

Reshaping $c_{(a_1,\sigma_2,...,\sigma_N)}$ into $\Psi_{(a_1,\sigma_2),\sigma'}$ once more, we apply the SVD and simplify similarly as before

$$c_{\sigma_1,\sigma_2,...,\sigma_N} = \sum_{a_1}^{r_1}\sum_{a_2}^{r_2} A^{\sigma_1}_{a_1} U_{(a_1,\sigma_2),a_2} S_{a_2,a_2} V^{\dagger}_{a_2,\sigma'} = \sum_{a_1}^{r_1}\sum_{a_2}^{r_2} A^{\sigma_1}_{a_1} A^{\sigma_2}_{a_1,a_2} c_{a_2,\sigma_3,...\sigma_N}.$$

The second A tensor that appears, that comes from a reshaped $U_{(a_1,\sigma_2),a_2}$, can be viewed as a set of d matrices of size $(r_1 \times r_2)$ and once more the singular values were absorbed into reshaped V tensor. Repeating this N times, we arrive at the final decomposition of the many body coefficient

$$c_{\sigma_1,\sigma_2,...,\sigma_N} = \sum_{a_1,a_2,...,a_N} A^{\sigma_1}_{a_1} A^{\sigma_2}_{a_1,a_2} \dots A^{\sigma_{N-1}}_{a_{N-2},a_{N-1}} A^{\sigma_N}_{a_N}$$

where for a given σ_i, A^{σ_1} is a matrix of size $(r_{i-1} \times r_i)$ with the exception of first and last tensors which are just vectors. If we suppress the bond indices and assume that the summation over them is implicit, our many body state in (2.1) is in a *matrix product state* (MPS) form

$$|\psi\rangle = \sum_{\sigma_1,\sigma_2,...,\sigma_N} A^{\sigma_1} A^{\sigma_2} \dots A^{\sigma_{N-1}} A^{\sigma_N} |\sigma_1, \sigma_2, ..., \sigma_N\rangle. \tag{2.5}$$

The σ_i indices are called the *physical* or *site* indices since they are directly related to a physical quantity while the bond indices are, in some sense, virtual degrees of freedom. In this work we will stick to the convention that upper indices are physical, while lower indices are bond indices. This decomposition is possible for any many body state on a lattice of N with a local Hilbert space of some dimension d. However, the matrices will grow exponentially in size, the largest being $(d^{\frac{N}{2}} \times d^{\frac{N}{2}})$ because the upper bound for the bond dimension is the lesser of the dimensions of the original matrix (assuming all singular values are retained) [12]. Therefore, this exact decomposition can be done for any state in theory, but not numerically, as the exponential growth would consume too much memory in practice for even modest spin size ($N = 28 - 32$).

2.2.2 Gauge Conventions

The A^{σ_i} matrices inherit some properties from the way we applied the SVD, in particular:

$$\begin{aligned}
\delta_{a_i,a_j} &= \sum_{(a_{i-1},\sigma_i)} (U^\dagger)_{a_i,(a_{i-1},\sigma_i)} U_{(a_{i-1,\sigma_i}),a_j} \\
&= \sum_{(a_{i-1},\sigma_i)} (A^{\sigma_i\dagger})_{a_i,a_{i-1}} A^{\sigma_i}_{a_{i-1},a_j} \\
&= \sum_{\sigma_i} (A^{\sigma_1\dagger} A^{\sigma_1})
\end{aligned}$$

which implies that

$$\sum_{\sigma_i} (A^{\sigma_i\dagger} A^{\sigma_i}) = \mathbb{1}. \tag{2.6}$$

Matrices satisfying this condition are called *left normalized* and is manifest only because we started from the 1st site in the lattice. We could have started from the right, at site N, and instead obtained

$$\sum_{\sigma_i} (B^{\sigma_i} B^{\sigma_i\dagger}) = \mathbb{1}$$

where the B^σ matrices are reshaped $V^\dagger$ matrices. The new matrix product state is essentially the same as (2.5), but now the matrices are right orthogonal. It is important to keep these normalization properties in mind when doing calculations analytically or numerically as in general it is not the case that the hermitian conjugate of each term in (2.6) sums to the identity. The literature refers to states containing only left or right normalized sets of matrices as *left* or *right canonical* states respectively. It is also possible to have a *mixed canonical* state where we decompose from the left up to some site n and decompose from the right, from site N, to site $n+1$ which yields a decomposition of $c_{\sigma_1,\sigma_2,\ldots,\sigma_N}$ into

$$c_{\sigma_1,\sigma_2,\ldots,\sigma_N} = A^{\sigma_1}A^{\sigma_2}\ldots A^{\sigma_n}\Lambda B^{\sigma_{n+1}}\ldots B^{\sigma_{N-1}}B^{\sigma_N}.$$

The A^σ matrices are left normalized while the B^σ are right normalized and the Λ matrix contains the singular values across bond $(n, n+1)$. This form is particularly useful when concerned with only two sites in the whole chain connected by a bond index and is closely related to the Schmidt decomposition of an MPS. One can quickly read off that [12]

$$|a_n^L\rangle = \sum_{\sigma_1,\ldots,\sigma_n} A^{\sigma_1}A^{\sigma_2}\ldots A^{\sigma_n}|\sigma_1,\sigma_2,\ldots,\sigma_n\rangle,$$
$$|a_n^R\rangle = \sum_{\sigma_{n+1},\ldots,\sigma_N} B^{\sigma_{n+1}}B^{\sigma_{n+2}}\ldots B^{\sigma_N}|\sigma_{n+1},\sigma_{n+2},\ldots,\sigma_N\rangle.$$

These can be used to write with Λ to write the whole state as

$$|\psi\rangle = \sum_{a_n=1}^{r_n} \Lambda_{a_n,a_n}|a_n^L\rangle|a_n^R\rangle$$

which is nothing but the Schmidt decomposition. The sum runs over a_n as the matrix products for the left ($|a_n^L\rangle$) and right ($|a_n^L\rangle$) states are vectors of size $(1\times r_n)$ and $(r_n\times 1)$ respectively which ensures that they respect the normalization conditions. For this reason, the bond at which the S matrix sits is called the center of orthogonality.

In general, there are many ways to establish normalization conditions, such as Vidal's $\Gamma\Lambda$ canonization [13], and their choice of application depends on what one would like to do with the state. This decomposition as we have just seen is not unique, we have already 3 different ways to arrive at an MPS form. One can transform each matrix with an invertible matrix U so that $A^{\sigma_i}\mapsto A^{\sigma_i}U$ and $A^{\sigma_{i+1}}\mapsto U^{-1}A^{\sigma_{i+1}}$ which leaves the matrix product invariant. The left, right and mixed canonical forms are ways to choose a "gauge" for our state.

2.2.3 Periodic Boundary Conditions

A subtle fact was implied when applying the MPS decomposition to the many body state in (2.1). It was assumed that the first site chosen and last site chosen were not connected, or in other words, that we had open boundary conditions. If instead we had some state with periodic boundary conditions such that there was a unit cell of N sites, the MPS form in (2.5) would need to be modified. In essence, all we have to change are the edge matrices as $A^{\sigma_1}_{1,a_1} \mapsto A^{\sigma_1}_{a_N,a_1}$ and $A^{\sigma_N}_{a_{N-1},1} \mapsto A^{\sigma_1}_{a_{N-1},a_N}$. Since the left and right indices are all that remain after performing the matrix product, the trace naturally appears

$$|\psi\rangle = \sum_{\sigma_1,\ldots,\sigma_N} \mathrm{Tr}(A^{\sigma_1}A^{\sigma_2}\ldots A^{\sigma_N})|\sigma_1,\sigma_2,\ldots,\sigma_N\rangle. \tag{2.7}$$

The intuition is that since the bond indices introduce "local interactions" between the sites, all we need to do is connect the first and last site the same way. Sometimes for numerical simplicity, the matrices throughout the chain can be taken to be uniform in size, even though in our derivation of the MPS form we allowed the matrices to take different sizes [12]. The reason is discussed below where we differentiate between an approximate MPS and an exact one. The state in (2.7) can also represent an translationally invariant system, where all the N A^{σ_i} matrices must be of the same size and comprise the unit cell.

2.2.4 Overlaps with MPS's

Once our state is in matrix product form, we can perform two key operations: overlaps of states and obtaining matrix elements (or expectation values as well) of operators. The former operation will inform us on how to perform the latter. Starting with two different MPS states with OBC, $|\psi\rangle$ and $|\phi\rangle$ with matrices C^σ and D^σ respectively, we can see that the overlap is simply

$$\langle\phi|\psi\rangle = \sum_{\sigma_1,\ldots,\sigma_N} D^{\sigma_N\dagger}\ldots D^{\sigma_2\dagger}D^{\sigma_1\dagger}C^{\sigma_1}C^{\sigma_2}\ldots C^{\sigma_N}. \tag{2.8}$$

The order in which this is carried out is important as performing the matrix product first and then the contraction over the site indices scales exponentially. One should first instead multiply the column vector $D^{\sigma\dagger}$ and row vector C^{σ_1} to form a matrix, and then sum over σ_1. At this point, we multiply the matrices either into $D^{\sigma_2\dagger}$ or C^{σ_2} and then contract over the site indices. The general idea is to keep multiplying matrices,

assumed to be of the same size $(n \times n)$ for the moment, which has a manageable computational complexity of $O(n^3)$. If not contracted correctly, the memory requirements would quickly render any calculation using an MPS numerically unwieldy. One can also quickly see that if our MPS $|\psi\rangle$ is in any of the three gauges shown, the state is naturally normalized, i.e. $\langle\psi|\psi\rangle = 1$.

By inserting an operator between the MPS's in (2.8) we can obtain matrix elements. It is important to note that in our standard form of our state, operators act on sites, which in the MPS language are the site indices of the matrices. Therefore, a single site operator O on site i must be of the form

$$O^i = \sum_{\sigma_i, \sigma_i'} O^{\sigma_i, \sigma_i'} |\sigma_i\rangle\langle\sigma_i'|.$$

Effectively, this will at most mix the the matrices in the MPS belonging to the same physical index. This results in the same computational complexity as the overlap of two states, as all that is different in (2.8) is the appearance of additional sums over σ_i over sites that support the operator.

2.2.5 Approximation of Ground States by MPS

It would seem that, in writing our many body state in an MPS form, we have simply introduced new degrees of freedom through the bond indices. A priori, there is no reason to assume that we are not drastically modifying our sate when we perform the decomposition and begin to mix the bond and site indices. We are by no means removing degrees of freedom, the typical approach in many body problems, but rather introducing artificial ones which does not solve our problem with the dimension of the many body Hilbert space. Namely, we are still faced with the issue of exponential growth of the matrices near the center of the matrix product. Moreover, we glossed over the difficulty in choosing an ordering of the lattice sites when performing this decomposition. On the surface it seems like this shouldn't matter too much, but already in two dimensions, one can see that there are many ways to separate out one site in a lattice. This choice of ordering can become very important as the scaling with N will suffer greatly numerically. Later on, we will discuss one particular method two try to circumvent this in two dimensional systems.

The concerns above are remedied by the following fact: The SVD is the best rank

deficient approximation of a matrix in the Frobenius norm [14]. That is, for a matrix M, there exists a matrix $\tilde{M}$ of smaller rank given by the SVD, where $\text{rank}(M) = \dim(\text{img}(M))$, such that

$$\left|\left|M - \tilde{M}\right|\right|_F$$

is minimized with $||M||_F = \sum_{i,j} M_{ij}^2$. The Frobenius norm is related to the L_2 norm of bipartite states $|\psi\rangle = \sum_{i,j} C_{ij}|a_i\rangle|b_i\rangle$ by

$$\left|\left|\,|\psi\rangle\right|\right|_2 = \sum_{i,j} |C_{ij}| = \left|\left|C\right|\right|_F$$

Therefore, the decomposition into a matrix product state can be seen as a rigorously justified *compression* of the many body tensor, $c_{\sigma_1,\sigma_2,\ldots,\sigma_N}$, into N rank 3 tensors, A^{σ_i}. One does not need to construct the MPS exactly for a given many body state $|\psi\rangle$, instead a cutoff χ can be chosen such that at each SVD, only at most χ singular values (or Schmidt states) are kept to some given tolerance $\epsilon(\chi)$. With these two parameters, we circumvent the issue of exponential growth of the matrices in the center of the MPS while keeping the most relevant states.

While it is possible to perform this decomposition in general for any many body state in any physical dimensions, the power of the MPS form is revealed only in low dimensional systems. In 1D, matrix product states can be easily formed by starting from the ends of the chain, and decomposing the many body tensor until one reaches the other side, since a linear chain provides a very simple ordering. More importantly however, it is possible to have very good approximations of the ground states of gapped systems. Such gapped states typically have rapidly decaying eigenvalues of $\rho_{A/B}$. As mentioned before, the Schmidt decomposition can be used to approximate any bipartite state and the mixed canonical form of the MPS is directly related to the Schmidt decomposition. Therefore, while performing this decomposition on a ground state of a gapped Hamiltonian, one can truncate the singular values retained during the SVD in order to reduce the sizes of the MPS matrices. One does this by specifying a maximum bond dimension χ, an upper bound on the size of the matrices within the MPS. The quality of the approximation for a gapped ground state $|\psi\rangle$ is given by [15]

$$\left|\left|\,|\psi\rangle - |\psi_{MPS}\rangle\right|\right|^2 \leq \sum_{i=1}^{N} \epsilon_i(\chi) \tag{2.9}$$

where $\epsilon_i(\chi)$ is the sum of the squares of the singular values at bond i for χ retained singular values. In other words, it is the sum of the truncation error in discarding the

unwanted singular values across each bond. If the singular values decay fast enough, χ can be small (10 to 50) but otherwise may be fairly large (200 - 1000). Since we only have a proxy of how the singular values behave in one dimension through (3), χ cannot be determined in advance. However, for large enough bond dimension, a suitable tolerance (10^{-8} to 10^{-10}) is typically possible. A poor convergence in this case would be when the discarded singular values are comparable in magnitude to those retained, which is often the case for gapless states.

2.2.6 The Transfer Matrix and Correlations

Matrix product states approximate gapped 1D states well due to entanglement reasons, but the behaviour of their correlations are also the same as gapped 1D states. A famous theorem from Hastings states that gapped ground states have exponentially decaying correlation, with some finite correlation length ξ, while gapless and critical states have power law correlations [16]. It is also the case that MPS's also have exponentially decaying correlations which is due strictly to their structure.

The key object that shows these decaying correlations is the transfer matrix. When performing the overlap $\langle\psi|\psi\rangle$ of an MPS, the following tensor appears often

$$T_i = \sum_{\sigma_i} (A^{\sigma_i})^*_{a'_1,a'_{i-1}} A^{\sigma_i}_{a_{i-1},a_i}. \tag{2.10}$$

This tensor is a rank 4 tensor that is typically reshaped into a matrix with new indices $(a_{i-1}a'_{i-1}, a_i a'_i)$, and called the transfer matrix. In the case of an translationally invariant MPS with an N unit cell, $\langle\psi|\psi\rangle$ yields

$$\langle\psi|\psi\rangle = (A^{\sigma_N})^*_{a'_N,a'_{N-1}} \dots (A^{\sigma_2})^*_{a'_2,a'_1} (A^{\sigma_1})^*_{a'_1,a_{N'}} A^{\sigma_1}_{a_N,a_1} A^{\sigma_2}_{a_1,a_2} \dots A^{\sigma_N}_{a_{N-1},a_N}.$$

By grouping the tensors by their physical indices, we can factor the overlap as

$$\begin{aligned}
\langle\psi|\psi\rangle &= (A^{\sigma_N})^*_{a'_N,a'_{N-1}} \dots (A^{\sigma_2})^*_{a'_2,a'_1} (A^{\sigma_1})^*_{a'_1,a_{N'}} A^{\sigma_1}_{a_N,a_1} A^{\sigma_2}_{a_1,a_2} \dots A^{\sigma_N}_{a_{N-1},a_N} \\
&= ((A^{\sigma_1})^*_{a'_1,a_{N'}} A^{\sigma_1}_{a_N,a_1})((A^{\sigma_2})^*_{a'_2,a_{1'}} A^{\sigma_2}_{a_1,a_2}) \dots ((A^{\sigma_N})^*_{a'_N,a_{N-1'}} A^{\sigma_N}_{a_{N-1},a_N}) \\
&= \mathrm{Tr}(T_1 T_2 \dots T_N).
\end{aligned}$$

The trace appears in the last line since, under an appropriate re-shape of the indices indicated above, the first and last matrices share an index. For simplicity, lets assume that all the A^{σ_i} matrices are similar (the general case for bigger unit cells is identical),

and suppose we decompose the single T matrix with the eigenvalue decomposition. Then, in its eigenbasis, the overlap is

$$\langle\psi|\psi\rangle = \mathrm{Tr}(T^N) = \sum_k (\lambda_k)^N.$$

Regardless of the normalization condition of the A matrix, for the state to be physical it must be normalized and therefore the overlap must be 1. In the thermodynamic limit, $N \to \infty$ and so it must be the case that $\lambda_1 = 1$ and $|\lambda_k| < 1$, $\forall k > 1$ otherwise the sum would not converge. The entries of A^{σ_1} may be complex, and hence so can the eigenvalues of T. The precise speed at which these eigenvalues must decay at determines how long range the correlations can be. To see this, we slightly modify the transfer matrix T_i in (2.10) by allowing an operator O_i to act on site i

$$T_i^{O_i} = \sum_{\sigma_i,\sigma_i'} O_i^{\sigma_i,\sigma_i'} (A^{\sigma_i})^*_{a_1',a_{i-1}'} A^{\sigma_i}_{a_{i-1},a_i}. \tag{2.11}$$

If we then want to calculate a two site correlation function

$$C(r) = \langle O_i O_j\rangle - \langle O_i\rangle\langle O_j\rangle, \tag{2.12}$$

with $r = |i-j|$, we need to use (2.11) in a similar way to how we did with the overlap of $|\psi\rangle$. If again we choose our MPS to have PBC and with all identical matrices for simplicity, the first term in (2.12) evaluates to

$$\langle O_i O_j\rangle = \mathrm{Tr}(T^{i-1}T^{O_i}T^{j-i-2}T^{O_j}T^{N-j-1}) = \mathrm{Tr}(T^{O_i}T^{j-i-2}T^{O_j}T^{N+i-j-2})$$

Inserting the resolution of the identity in terms of the eigenstates of T we have

$$\begin{aligned}
\langle O_i O_j\rangle &= \sum_{n,m} \langle n|T^{O_i}T^{j-i-2}|m\rangle\langle m|T^{O_j}T^{N+i-j-2}|n\rangle \\
&= \sum_{n,m} \lambda_n^{(N+i-j-2)}\lambda_m^{(j-i-2)}\langle n|T^{O_i}|m\rangle\langle m|T^{O_j}|n\rangle \\
&= \sum_{m} \lambda_m^{(j-i-2)}\langle 1|T^{O_i}|m\rangle\langle m|T^{O_j}|1\rangle
\end{aligned}$$

where in passing from the 2nd to the 3rd line, we used the fact that in the thermodynamic limit we expect the transfer matrix eigenvalues to be such that $\lambda_1 = 1$ while all others are $\lambda_i < 1$, which tend to zero. Letting $r = |i-j-2|$, $\xi_m = -1/\ln(\lambda_m)$, and $c_m = \langle 1|T^{O_i}|m\rangle\langle m|T^{O_j}|1\rangle$, we have the final asymptotic form

$$\langle O_i O_j\rangle = c_1 + \sum_{k=2} c_k e^{-r/\xi_k}. \tag{2.13}$$

The constant term in the front is canceled out from the second part of (2.12), as $\langle T^{O_i}\rangle\langle T^{O_j}\rangle$ contribute only $\langle 1|T^{O_i}|1\rangle\langle 1|T^{O_j}|1\rangle$ in the thermodynamic limit. The correlations can be long range provided the exponentials decay slowly enough and the matrix elements c_k are non zero. Therefore, MPS's turn out to be finitely correlated states, just like gapped 1D states of local Hamiltonian's. They can still approximate long range power law correlations well in critical systems as (2.13) can be made to sum over more exponentials by increasing the bond dimension which approximate the power law better [17, 18]. It is possible to construct a similar tensor network, the multi-scale entanglement renormalization ansatz, that naturally encodes longer range correlations capable of accurately approximating critical systems [18, 19]. These networks are beyond the scope of this work.

2.2.7 Matrix Product Operators

The last tool that we need to introduce is that of the matrix product operator (MPO) [20, 21]. Since we have now broken down our state into MPS form, we need to find a way to calculate the action of the Hamiltonian, and hence general operators, on our state. The MPS is written such that each matrix in (2.5) encodes information about a single site and how it interacts with neighboring sites. The MPO therefore, must also act on the single site and can only do so via the physical index of the matrix. A form that would satisfy these conditions for an operator O is

$$O = \sum_{\sigma,\sigma'} W^{\sigma_1,\sigma_1'} W^{\sigma_2,\sigma_2'} \dots W^{\sigma_N,\sigma_N'} |\sigma\rangle\langle\sigma'| \tag{2.14}$$

where $\sigma = \sigma_1, \sigma_2, \dots \sigma_N$. The $W^{\sigma_i,\sigma_i'}$ matrices have two hidden bond indices that are implicitly summed over, making them rank 4 tensors. Every operator can be written in MPO form but not uniquely, just like an MPS. This is typically done with some convention, but the overall goal is take one and two body operators and place them correctly in matrices, ensuring that their product correctly accumulates the operators. Acting only on the physical indices, an MPO - MPS multiplication returns another MPS as seen by looking at only one contraction:

$$\sum_{\sigma_i} W^{\sigma_i,\sigma_i'}_{b_{i-1},b_i} A^{\sigma_i}_{a_{i-1},a_i} = (WA)^{\sigma_i'}_{a_{i-1},a_i,b_{i-1},b_i} = (WA)^{\sigma_i'}_{(a_{i-1},b_{i-1}),(a_i,b_i)} \equiv C^{\sigma_i'}_{c_{i-1},c_i}.$$

While the matrix dimension has gone up, precisely by the product of the dimensions of the bonds of $W^{\sigma_i,\sigma_i'}$ and A^{σ_i} , the new C^{σ_i} form can be applied to all matrices in the MPS. In practice, one does not just apply one operator on a state, instead expectation

values are obtained. One can see that this looks very similar to how single site operators were introduced in the sections above. The difference here is that we are inherently dealing with sums and product of operators. Each $W^{\sigma_i,\sigma_i'}$ is a matrix containing operators on site i, while before the O_i operators were single site operators. The MPO is a very clean way to sum over the spin indices in one object that overall acts like a quantum mechanical operator. The power of the MPO formalism will be more evident when discussing variational ground state searches with an MPS.

It must noted that this entire time we have only discussed our ability to approximate gapped ground states *provided* that we actually have the state. As mentioned before, it is not a simple task to obtain ground states of spin systems and this remains our primary goal. All we have shown so far is that provided our Hamiltonian is gapped and local, its ground state can be approximated by a matrix product state. To *obtain* said approximate state, one needs a method to variationally optimize a trial wave function in matrix product state form. However, in light of the mixed Canonical form, we have the ability to single out two sites, across some bond n, out of our whole lattice. The bonds could then be optimized before moving the center of orthogonality over and repeating the process. This is goal of the next section, were we introduce the density matrix renormalization group and how it can be used to optimize our MPS's.

2.3 The Density Matrix Renormalization Group

In 1992, White proposed the original formulation of the density matrix renormalization group as a way to solve for the ground state of quantum chain [22]. The main idea was to iteratively add in two sites and solve for the ground state of the chain in a particular product form. The was made possible by using the reduced density matrix at each step to retain the most "important" states while enlarging the system. As the process of changing the scale of the system and integrating out marginal degrees of freedom is commonly referred to as renormalization, the whole procedure was named the density matrix renormalization group (DMRG).

2.3.1 MPS formulation of DMRG

As DMRG grew in popularity due to its power and accuracy, it has since been reformulated as a variational method on MPS's due to their intimate link to 1D systems. The modern version of DMRG is a method to find the ground state $|\psi\rangle$ in MPS form of some

1D Hamiltonian H by minimizing the energy [12]. Specifically, we seek to extremize

$$\langle\psi|H|\psi\rangle - \lambda\langle\psi|\psi\rangle$$

where λ is a Lagrange multiplier. If $|\psi\rangle$ is in MPS form (in open boundary conditions) with matrices A^σ, for some site i, the matrix A^{σ_i} can be optimized via

$$\frac{\partial}{\partial(A^{\sigma_i})^\dagger}(\langle\psi|H|\psi\rangle - \lambda\langle\psi|\psi\rangle).$$

When performing the calculation efficiently, by keeping the optimal order of contractions when applying H (assumed to be in MPO form), the optimization of matrix A^{σ_i} is equivalent to the eigenvalue problem [12]

$$\sum_a M_{a,a'}(A^{\sigma_i})_a = \lambda(A^{\sigma_i})_{a'}$$

where $a = a_{i-1}a_i\sigma_i$ is a reshaped index so that $A^{\sigma_i}_{a_{i-1},a_i}$ is reshaped into a vector. The $M_{a,a'}$ is the contraction of the network of tensors:

$$M^{\sigma_i,\sigma_i'}_{a_{i-1},a_{i-1}',a_i,a_i'} = (A^{\sigma_1}_{a_1}\dots A^{\sigma_{i-1}}_{a_{i-2},a_{i-1}} A^{\sigma_{i+1}}_{a_i,a_{i+1}}\dots A^{\sigma_N}_{a_{N-1}})^\dagger (H^{\sigma_1,\sigma_1'}_{h_1}\dots H^{\sigma_i,\sigma_i'}_{h_{i-1},h_i}\dots H^{\sigma_N,\sigma_N'}_{h_N-1}) (A^{\sigma_1}_{a_1}\dots A^{\sigma_i}_{a_{i-1},a_i}\dots A^{\sigma_N}_{a_{N-1}}).$$

Effectively, the $(A^{\sigma_i})^\dagger$ tensor is removed, so the reshaped $M_{a,a'}$ acts on a vectorized version of A^{σ_i}. It must be emphasized that this contraction must be done efficiently otherwise the memory usage when implemented numerically would make this method intractable. This eigenvalue problem is solved by some ground state eigensolver, typically a Lanczos method, and the matrix is then updated. The process occurs in *sweeps*: starting from $n = 1$, the optimization is done to each next site in the chain until reaching $n = N$ and then performing it once more on the way back to site $n = 1$. At each eigenvalue step, the SVD is employed to impose the desired orthogonality conditions on the matrices and truncate the singular values to some desired maximum bond dimension χ. While seeming quite different than the original formulation, the density matrix is still the deciding factor as the singular values are directly related to the eigenvalues of the reduced density matrix. It is also possible to also calculate some excited states of H by adding in penalty term to the Hamiltonian [23]

$$H \to H + P|\psi_0\rangle\langle\psi_0|$$

where $|\psi_0\rangle$ is the ground state obtained through DMRG. In the basis of the eigenstates of the H, this shifts the spectrum so $E_0 \to E_0 + P$. If P is large enough, at least the size of the gap, then we must have that $E_1 < E_0 + P$. By running DMRG once more on this new Hamiltonian, yields the first excited state as we have "pushed" the ground state up so as to not be the lowest state anymore.

2.3.2 Infinite DMRG

The procedure discussed above is related to, but not directly similar to the original formulation by White. Now referred to as finite DMRG, the method focuses on a variational method in the space of matrix product states on N sites. The original proposal by white consisted of growing a system until it reach a fixed point in a renormalization sense which seems lost in the modern finite scheme. While finite DMRG can probe easily several hundred sites to great accuracy, it ultimately cannot obtain results in the thermodynamic limit without extrapolating finite sized results. Luckily there exists an infinite sized version that can obtain a translationally invariant MPS in the form of (2.7), for a given unit cell size, which can access the thermodynamic limit.

Staying closer to White's first proposal, infinite sized DMRG (iDMRG) looks to insert a unit cell in the center of the chain iteratively until the MPS is unchanged [24]. Starting with only 2 unit cells of size N_u each, the ground state is obtained using finite DMRG and then a unit cell is inserted between the two unit cells. This new enlarged wavefunction is the initial guess for the ground state of the $3N_u$ chain. Since the goal is to create a translationally invariant state, only the inserted tensors get optimized, while the previous tensors from the two unit cell calculation, called the left and right environment block, are untouched. The inserted tensors will be optimized via finite DMRG under a suitable choice of Hamiltonian of the entire $3N_u$ chain, referred to as the super block Hamiltonian. By projecting onto the inserted unit cell Hilbert space, the environment blocks help form an effective Hamiltonian on the N_u sites that can be used to optimize their matrices. The process is repeated until the density matrix across the center site becomes a fixed point.

The main difficulty in implementing an efficient version of the algorithm stems from the choice of the tensors to insert into the state at each step. A careful choice should be taken as it can provide a large performance gain during the Lanczos step of the finite DMRG. The main idea, as proposed in [24] is to insert, taking a two site unit cell, the following unit cell in mixed canonical form at step n

$$A^{\sigma_1}_{[n]}\Lambda_{[n]}B^{\sigma_2}_{[n]}\Lambda^{-1}_{[n-1]}, \tag{2.15}$$

where the subscript refers to the nth step, A and B are in the left and right gauges, and Λ is the center of orthogonality that holds the singular values. An equivalent version to this [25] is to insert one unit cell into each environment block after each step, keeping the

previously obtained N_u matrices in the center. Then, the super-block Hamiltonian is reconstructed and finite DMRG is ran once more, the goal being to optimize the bonds between the ends of the center unit cells and the new parts of the environment blocks. In either case, the subtlety lies in how exactly one choose to optimize the matrices best so as to mimic translationally invariant conditions without making the sizes too large. The output in both cases, should be an translationally invariant approximation to the ground state of the Hamiltonian in the thermodynamic limit.

2.3.3 Why DMRG Works So Well

In one dimensional systems, DMRG excels at finding ground states of interacting systems. As mentioned before, due to the efficient compression of matrix product states, gapped states are particularly well approximated and obtained by DMRG. In both finite and infinite methods, the ability to truncate the singular values (or equivalently the eigenvalues of the reduced density matrix) during the sweeps makes the method computationally efficient and accurate. While in general one cannot know the spectrum, even for several hundreds of retained singular values, the approximations can become very good.

A less rigorous argument can also be made via the area law. Suppose we have to d dimensional subsystems A and B that are maximally entangled. Then, the eigenvalues of the reduced density matrix λ_i must all be equal with value $1/d$, giving an overall bipartite entanglement entropy of

$$S_{AB} = -\sum_{i=1} \frac{1}{d} \ln(\frac{1}{d}) = \ln(d).$$

In 1D for gapped states, S is bounded by some constant $\tilde{S}$ so that $\ln(d) \leq \tilde{S}$, or in other words $d \leq e^{\tilde{S}}$. That is, there is a constant upper bound, in principle, on the bond dimension that would be optimal in retaining all important singular values given some maximal entropy $\tilde{S}$. This argument fails in 2D and 3D as the bound changes to e^N and e^{N^2} respectively, leading to exponential increases in the memory required to store the MPS. One can still probe *quasi*-2D systems, several chains glued together for example, with decent success [23]. The primary hurdle faced is the increasing number of longer ranged interactions between sites which decrease the sparsity of the MPS matrices.

2.4 Symmetry protected topological phases

A large part of condensed matter physics is concerned with understanding and classifying phases of solid state materials. In the context of quantum theory, it is also possible for quantum systems to undergo a *quantum* phase transition (QPT) by varying the strength of the interactions between the particles. The primary way phase transitions were understood in general, was the concept of symmetry breaking, initially proposed by Landau [26]. The idea is that when undergoing a transition at some value of a particular parameter, the two phases ultimately differ in what symmetries they support and must be broken across the transition point. Based on the symmetries, an *order parameter* is chosen that tracks a quantity that should change sufficiently across the transition point. For example, in the Ising model, one can use the magnetization m of the state as a measure of "order" in the state. In the high temperature regime, the model is disordered due to the spins being randomly oriented yielding $m = 0$ called the disordered state. When lowering the temperature, the spins begin to align past some critical temperature T_c with magnetization $m = \pm 1$ and become ordered. Whether the magnetization is positive or negative is completely random and can be understood through symmetry breaking. In the disordered phase, the order parameter has Z_2, or spin-flip, symmetry and hence the energy of the state should not change under such an operation. However, in the ordered state, if $m = 1$ then all the spins are aligned pointing up, meaning that a global spin flip would change the magnetization to $m = -1$. Therefore, we say that the Z_2 symmetry is broken in the ordered phase as it is does not respect the symmetry of the system below a certain a critical temperature.

The symmetry breaking paradigm is very powerful and explains a large amount of phase transitions, including quantum ones. In general, the breaking of symmetries mean that the ground state is invariant under a *subset* of the symmetry group G_H of the Hamiltonian. In the Ising model example $G_H\{1, \in\}$ and so the broken symmetry in the ordered phase is simply $G_O = \{1\} \subset G_H$. However, it turns out that it is possible to undergo a phase transition *without* breaking any symmetries. An example of this is manifest in the Spin-1 Haldane chain [27],

$$H = J \sum_i \mathbf{S_i} \cdot \mathbf{S_{i+1}} + D \sum_i (S_i^z)^2 \tag{2.16}$$

With $D \geq 0$ and $J > 0$. For $D = 0$, the Hamiltonian is just the spin-1 Heisenberg antiferromagnet, who's ground state is gapped but does *not* break any symmetries of the Hamiltonian [3, 28] . As D is increased, the ground state undergoes a transition to

another gapped phase at $D \approx 1$ which also does not break any symmetries called the large D phase [29, 30]. In order to understand such transitions, we need to employ a new formalism that can differentiate the two phases.

2.4.1 Classifying Quantum Phases of Matter

Before proceeding we need to briefly explain how phase transitions are understood for gapped ground states of quantum systems. The most intuitive definition is that two gapped ground states are said to be in the same phase if they can be adiabatically connected by varying a parameter in their Hamiltonian without the gap closing [31–33]. The fastest way to determine if a gapped state undergoes a phase transition is to see if its gap closes, if the gap remains non zero through the adiabatic evolution, no phase transition has occurred. The more formal definition is that two gapped ground states are in the same phase if and only if they are can be mapped into one another under a finite number of local unitary operations [32]. Effectively, this would mean in both cases that states are in the same phase if the are essentially the same except they may contain slightly more or less entanglement locally than one another. This also means that product states, which have no entanglement and states with some local entanglement are effectively the same and belong to the same phase. If the states cannot be connected adiabatically, then the states are said to be in different phases.

2.4.2 Defining Features of SPT Phases

The local unitary prescription for understanding quantum phase transitions is difficult to use in practice but useful in concept. One must construct a path in the space of Hamiltonians from local unitary operators in order to show that the ground states belong to the same phase. In principle, allowing any such path makes this task straightforward, but when further imposing the path to respect the symmetries of the initial Hamiltonian, some further structure emerges. In this restricted set of paths, it will be possible to have two ground states that respect the same symmetries, but along some path connecting them undergo a transition, i.e. the gap closes. The phases that host these states are called *symmetry protected topological* (SPT) phases primarily because they are only possible when these symmetries are present, hence "protecting" the phase. They are also called topological because depending on the boundary conditions, or in other words the geometry, they may host edge modes, localized gapless states at the edges of the system. We will look at exactly how such a phenomenon occurs in spin

chains in the next sections. SPT phases are also present in non interacting fermionic systems, a notable example being the topological insulator which is protected by time reversal symmetry [34].

2.4.3 Projective Representations

In 1D, SPT phases can be understood through the matrix product state formalism as they approximate gapped ground states naturally and efficiently. To understand how the invariance under the symmetry group G_H of the Hamiltonian H effects our ground state, we must first understand the action of the symmetry group on an MPS. For $g \in G_H$, the action of g on a state $|\psi\rangle$ is

$$|\phi\rangle = \prod_m u^m(g)|\psi\rangle, \tag{2.17}$$

where $u^m(g)$ is the linear representation of the element g acting on site n. If $|\langle\phi|\psi\rangle| = 1$ for all $g \in G_H$, then the state $|\psi\rangle$ is invariant under the group G_H and shares the same symmetries as H. It important to stress here that the $u^m(g)$ form a linear representation of the group G_H. If the state is in MPS form then the $u^m(g)$ act solely on the physical indices of the matrix as, in general, they know nothing about the bond indices. Crucially, under a symmetry operation the A^{σ_i} matrices transform as [35]

$$\sum_{\sigma_i} u^m_{\sigma_i\sigma_j}(g)A^{\sigma_i} = e^{i\theta_g}U^\dagger(g)A^{\sigma_j}U(g) \tag{2.18}$$

where $e^{i\theta_g}$ is a phase and $U(g)$ is a unitary matrix that acts on the bond indices. The $U(g)$ are said to form a *projective* representation of the symmetry group G_H. That is, for two group elements $g_1, g_2 \in G_H$ we have that

$$U(g_1)U(g_2) = \omega(g_1, g_2)U(g_1g_2)$$

where the $\omega(g_1, g_2) \in U(1)$ are phases that form the so called factor set of G_H. The phases can be changed upon some re scaling $\tilde{U}(g) = \beta(g)U(g)$, yielding

$$\tilde{\omega}(g_1, g_2) = \frac{\beta(g_1g_2)}{\beta(g_1)\beta(g_2)}\omega(g_1, g_2). \tag{2.19}$$

The two projective representations are said to be equivalent if the factor sets are in the same equivalence class if (2.19) is the equivalence relation. These different classes distinguish the possible kinds of projective representations one can get from a given group G. In more precise terms, the equivalence class of factor sets are the second

cohomology group $H_2(G, U(1))$ of G [36]. The upshot from this is that the phase factors, the ω, cannot be gauged away trivially and can be used to index which projective representation is present.

The linear representation acting on the physical indices of an MPS yields a projective representation that acts on the A^σ matrices. Coupled with the fact that the MPS should be invariant under the symmetry group, we have enough information to classify the SPT phases. The key tool will be the transfer matrix, which will be able to actually obtain the $U(g)$ matrices provided we know the symmetry group G_H.

2.4.4 The Mixed Transfer Matrix

If our MPS is to be invariant under the symmetry group, the overlap with the untransformed version should be equal to 1. As is common with overlaps of matrix product states, one must examine the transfer matrix in the infinite limit. However, the standard expression in (2.10) must be suitably modified to

$$T_i(g) = \sum_{\sigma_i} \sum_{\sigma_k} (A^{\sigma_i})^*_{a'_1, a'_{i-1}} (u^m_{\sigma_i \sigma_k}(g) A^{\sigma_k}_{a_{i-1}, a_i}), \tag{2.20}$$

which is called the *mixed* transfer matrix. While not mentioned before, the normalization conditions of the matrices used in the formation of the transfer matrix impose conditions on their eigenvectors. It must still remain true in the thermodynamic limit the dominant eigenvector must have as its dominant eigenvalue $|\lambda_1| = 1$ (the norm is included as the transfer matrix is not hermitian.). If the matrices comprising T_i are left normalized, then the left eigenvector V is such that $VT_i = V$, while if they are right normalized then $T_i V = V$ [37]. The V eigenvector must also be the identity in both gauges as otherwise the overlap would not in general be $= 1$.

One can show using (2.20) and (2.18) that the transfer matrices constructed from left (right) normalized matrices are such that the dominant left (right) eigenvector of $T_i(g)$ is precisely $U(g)$ [38]. The idea is that in the thermodynamic limit, the transfer matrices are connected such that the $U(g)$ and $U^\dagger(g)$ matrices will cancel out across the bond indices. The transfer matrices are then contracted infinitely yielding only a single $U(g)$ matrix on the right (left) bond from where the contraction was started. Comparing with the product of transfer matrices from just (2.20) we must conclude that the dominant eigenvector (typically normalized) is the $U(g)$ itself.

Once the $U(g)$ are all obtained, one can extract the factor set of the group and determine which projective representation the phase is in. Depending on the group structure, certain elements may or may not commute and products can be formed of the group elements such that the $\omega(g_1, g_2)$ phase can be isolated. Typically, phases can be gauged away under a suitable re-scaling but as we will see in the next section it is possible to make extract a gauge *invariant* phase.

Under this formalism, all 1D SPT phases can be classified based on the possible symmetry groups that the systems can have in 1D [32,36,39]. One first looks at the symmetry group G of the system and then can either calculate or consult the literature on how many projective representations G admits. The number of projective representations of G is the maximum possible number of SPT phases allowed in the model. To determine which phase the ground state is in, one needs to extract the projective representations $U(g)$ for $g \in G$ and form gauge invariant combinations. This will be done for the Haldane chain in the next section.

2.4.5 Spin-1 Haldane Chain and SPT Classification

To demonstrate how the SPT formalism works, we will use the Spin-1 Haldane Chain (2.16) and classify the two gapped non symmetry breaking states.

Firstly, in the $D = 0$ the ground state is in the Haldane phase, gapped, and disordered. While this ground state is hard to obtain analytically, it has been shown numerically to be adiabatically connected to ground state of the AKLT model [37]. The AKLT Hamiltonian is another spin-1 system similar to the Haldane chain, it is given by [40]

$$H = \sum_i \mathbf{S_i} \cdot \mathbf{S_{i+1}} + \frac{1}{3}(\mathbf{S_i} \cdot \mathbf{S_{i+1}})^2. \tag{2.21}$$

The ground state can be written down exactly as an MPS (REF) in the form of (2.5) with matrices M^σ [12]

$$M^+ = \begin{pmatrix} 0 & 0 \\ \frac{-1}{\sqrt{2}} & 0 \end{pmatrix}, M^0 = \begin{pmatrix} \frac{1}{2} & 0 \\ 0 & \frac{-1}{2} \end{pmatrix}, M^- = \begin{pmatrix} \frac{1}{\sqrt{2}} & 0 \\ 0 & 0 \end{pmatrix}. \tag{2.22}$$

The intuition is that the spin-1 at each site can be projected to 2 spin-1/2 that form singlets with the neighboring sites (See Fig. **??**). Because of this *fractionalization* of the spins, it is possible in open boundary conditions to cut a singlet in half, leaving 2 free spin-1/2 at the ends of the open chain leading to a 4-fold degeneracy of the ground

state. The MPS form in (2.22) is just an exact and cleaner way to codify this into a wavefunction, which can also be done by taking the tensor product of various spin-1/2 singlets and then projecting back to the total spin-1 sector [40]. When $D \geq 1$, the ground state of (2.16) can be connected to a trivial product state $|\psi_{GS}\rangle = \prod_i |0\rangle_i$ called the large D phase [37]. This makes sense as in the limit where $D \to \infty$, this is the state with the lowest energy.

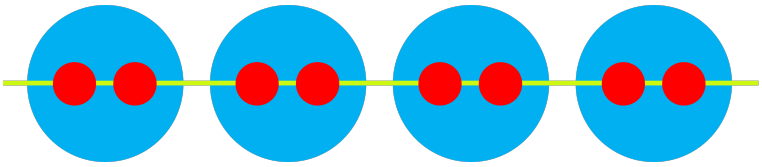

Figure 2.2: Schematic of the Haldane chain where the blue circles indicate a spin 1 site, the red circles are spin 1/s particles and the green line connecting them are singlet nearest neighbor bonds. One can see that the spin 1/2 particles at the edges are left uncoupled at the edges of the chain, while the bulk spin 1/2's are paired up as singlets.

Using the AKLT ground state and the product state to represent the Haldane phase and the large D phase respectively, we can classify these phases using the SPT formalism. A symmetry respected by (2.16) is the dihedral group $D_2 = \{1, R_x, R_z, R_x R_z\}$, where R_x is a π rotation about the x axis and R_z is rotations about the z axis. Other symmetries can be used to form an index like time reversal and inversion, but we will chose to work with rotations. Once can show that a gauge invariant product can be formed via [37, 38]

$$U(R_x)U(R_z)U^\dagger(R_x)U^\dagger(R_z) = \pm 1. \tag{2.23}$$

The $+1$ corresponds to the large D phase and -1 is the Haldane phase. The Haldane phase therefore shows non trivial commutation relations and has non trivial $U(g)$ matrices which form a projective representation. This can be seen due to the edge modes being spin-1/2 which have non trivial behaviour under rotations: $R_z R_x|+\rangle = -|-\rangle$ while $R_x R_z|+\rangle = |-\rangle$. Since the large D phase is a product state of spin-0 it transforms trivially under D_2 and therefore has a trivial abelian representation. Unless the symmetry group is broken during the transition from $D = 0$ to $D \geq 1$, the Z_2 index in (2.23) is robust and identifies the phases clearly.

The main idea when trying to extract the $U(g)$ matrices is that when when acting with a symmetry operation on a site the $U(g)$ matrices appear as a similarity transfor-

mation of the A^σ matrices, like in eqt. 2.18. To extract the $U(g)$ matrices, one needs to look near an edge of a chain of some kind as chaining two neighboring matrices, that have undergone the same symmetry operation, will cancel the $U(g)$ matrices between them as they always contract with their inverse. Therefore, only matrices left at the edges remain.

2.4.6 Presence of Degeneracy in the Entanglement Spectrum

The spectrum of the reduced density matrices, sometimes also referred to as the entanglement spectrum, provide a useful indicator of the presence of SPT phases. If a state is to be protected by a symmetry group G, meaning it cannot be then it has a projective representation of its elements $U(g)$. Because of the complex phase that appears in the group multiplication, we can find elements that do not commute, like in (2.23). The reduced density matrices $\rho_{A/B}$ across any bipartition will commute with each of the group elements trivially because the group elements leave the wavefunction invariant. From Shur's lemma in representation theory, we know that an operator O that commutes with a group representation that is non abelian means that the irreducible representations must have dimensions larger than 1, yielding degeneracies in the eigenvalues of O. This means that the entanglement spectrum must be degenerate, precisely how depends on the symmetry group. In the Haldane chain for example, there is an exact doubling of the eigenvalue of $\rho_{A/B}$ [37].

It is important to note that the degeneracies in the entanglement spectrum are a signature of an SPT. They do not in general inform us of which projective representation is present in a given phase. However, once the phase has been classified according to an index, they tracking the degeneracy of the entanglement spectrum can be very useful when studying the phase in question. For example, when studying the stability of an SPT phase by slowly breaking the symmetry that protects the SPT phase with a perturbation, one can track the difference in the entanglement spectrum $|\lambda_1 - \lambda_2|$ in the case that λ_1, λ_2 are degenerate. As the symmetry breaking perturbation gets larger, the difference between the eigenvalues can become non zero, indicating that a phase transition.

Chapter 3

Kitaev Spin Systems

In this section we introduce the Heisenberg Gamma ($J-\Gamma$) ladder and discuss its origin. We begin by discussing the Kitaev Honeycomb model, an exactly solvable model that hosts anyonic excitations forming a so called Kitaev spin liquid. From there, we discuss the experimental feasibility and known materials that are candidates to host the exotic phase. Then, we explain that several interactions are present in real materials, such as the Heisenberg and Gamma interactions that are present in candidate materials at low temperature. To study the possible phases admitted by these interactions, we attempt to section off parts of the complete Kitaev-Heisenberg-Gamma phase diagrams in an effort to understand the role of individual interactions. We then introduce the Heisenberg-Gamma ladder and discuss its important features.

3.1 The Kitaev Honeycomb Model

In 2006, Kitaev brought forth an anisotropic interacting spin-1/2 model on a honeycomb lattice. The remarkable fact about the model is that its exactly solvable and hosts non-abelian*anyonic* excitations, particles that have non trivial exchange statistics. The model is given by [41]

$$H = -K_x \sum_{x-\text{links}} \sigma_j^x \sigma_k^x - K_y \sum_{y-\text{links}} \sigma_j^y \sigma_k^y - K_z \sum_{z-\text{links}} \sigma_j^z \sigma_k^z \tag{3.1}$$

where σ_j^α are the Pauli matrices and the $x, y,$ and$z$ links are depicted in (Insert figure). The spin interactions are anisotropic and have competing Ising like interactions, making (3.1) difficult to diagonalize. One can notice that an operator W_p can be defined for a given plaquette p of the honeycomb lattice

$$W_p = \sigma_1^x \sigma_2^y \sigma_3^z \sigma_4^x \sigma_5^y \sigma_6^z. \tag{3.2}$$

These so called plaquette operators come from looking at the remaining link dangling from the ith site situated in plaquette p. Miraculously, it turns out that $[H, W_p] = 0$ for all p, which we will exploit heavily since it simplifies our problem greatly. Moreover, plaquettes operators commute as long as the plaquettes are not the same $[W_p, W_p'] = 0$ and when applied twice yields the identity $W_p^2 = 1$. This means that the total Hilbert space splits into different sectors of different W_p eigenvalues who that can only take on values of $w_p = \pm 1$. The unit cell of the Honeycomb lattice contains 2 spins, so for N unit cells, the Hilbert space is of size 2^{2N}. There are N plaquettes so the original Hilbert space dimension gets reduced to $2^{2N}/2^N = 2^N$, which is still exponentially large. One can then express our on site spin-1/2 fermions as majorana's

$$c_{2j-1} = a_j + a_j^\dagger, \quad c_{2j} = \frac{a_j - a_j^\dagger}{i} \tag{3.3}$$

where $a_j, a_j^\dagger$ destroy and create a fermion at site j and c_j are the majorana fermion operators. A single fermion creates two majorana fermions, which are their own annihilating particle $c_j = c_j^\dagger$ and $c_j^2 = 1$. For each spin at the vertex of the lattice, which has local Hilbert space dimension 2, we represent it by 4 majorana fermions (two for each spin choice) defined by

$$\tilde{\sigma_j}^x = i b_j^x c_j, \quad \tilde{\sigma_j}^y = i b_j^y c_j, \quad \tilde{\sigma_j}^z = i b_j^z c_j. \tag{3.4}$$

The tildes denote that the $\tilde{\sigma_j^\alpha}$ act on a 4 dimensional space, rather than the original one of size 2 which is now a subspace. The b_j^x, b_j^x, b_j^x, c_j majorana operators can be interpreted physically when they are projected back into the 2 dimensional subspace. This is done by enforcing two conditions on the augmented space. Firstly, the $\tilde{\sigma_j^\alpha}$ need to obey the correct commutation relations of the pauli matrices within the physical subspace. Secondly, the state has eigenvalue 1 of the operator $D_j = b_j^x b_j^y b_j^z c$. the reason for this is that $\sigma^x \sigma^y \sigma^z = i$ in the spin-1/2 algebra, hence we should also expect $\tilde{\sigma}^x \tilde{\sigma}^y \tilde{\sigma}^z = i$ as well in the physical subspace. In some sense, this fixes the gauge of the spin representation of the operators and can be used a way to project into the physical subspace.

Under this transformation, the plaquette operators and the Hamiltonian can be written as a quartic sum of the majorana operators. In principle, we would have to calculate the ground state in each W_p sector and then choose the lowest one. However, according to a theorem by Lieb [42], the ground state must be such that $W_p = 1$ for all p. Kitaev showed that there are two possible phases, named A (gapped) and B (gapless), depending on the values of the coupling constants K_x, K_y, K_z. The gapped phase can

be related to and understood via the toric code model, which host non-local anyonic excitations that create topological order [43]. These anyonic excitations are particles that are neither bosonic, or fermionic, they instead accrue a phase factor $e^{i\theta}$ upon exchange. The gapless phase, when made gapped under a time reversal breaking perturbation, can host so called non-abelian anyonic excitations and displays robust chiral edge modes [41]. Note that the symmetry broken version of the B phase cannot be done exactly and must be done perturbatively or numerically.

Phase B, when made gapped, will have decaying spin correlations functions and hence shows no particular magnetic ordering (Need a ref). A quantum state that show no magnetic ordering while being strongly correlated is referred to as a quantum spin liquid (QSL). This definition is slightly contentious as it states what a QSL isn't, namely a magnetically ordered strongly interacting phase. A more apt definition would also involve the fact that these QSL are highly entangled states and potentially show topological (non local) order [44, 45]. Hence, the broken time reversal B phase is sometimes referred to as a Kitaev spin liquid. In general, the strongly correlated spin systems are very difficult to solve exactly, the Honeycomb model being an exception. This is where the strength of DMRG and similar Tensor Network methods really shine as they efficiently approximate the ground states for 1D and quasi 2D strongly correlated systems.

It was shown that non abelian anyons can be used for fault tolerant quantum computation [43]. As the primary property of anyons is related to the phase gained when exchanging them, the main tool used to understand anyons is their braid group. This is the set of equivalence classes of trajectories of particles equipped with a "braiding" operation where two trajectories are intertwined [46]. A non abelian anyon has a non abelian braid group and an abelian anyon has an abelian braid group. The benefit of using anyons as qubits for quantum computation is that the anyons only change when braided, making them robust to perturbations and are an attempt to mitigate issues caused by decoherence [47].

3.2 The Kitaev Interaction in Materials

The non-abelian anyons present in the Honeycomb ladder make it an exciting and worthwhile system to study and try to realize experimentally. In 2008, it was shown that Mott-Hubbard systems with electron-electron interactions and strong spin orbit coupling could host Kitaev like interactions [48]. The transition metals are known to

have strong spin orbit coupling that effectively localises the electrons, and those that have octahedra like the iridates can give rise to bond dependent spin exchanges. The octahedra can share a corner through a mediating O atom which leads to a single spin super exchange between two Ir atoms, effectively forming a Heisenberg interaction [49]. However, if the octahedra share an edge instead, two super exchange paths can be formed which interfere with one another, canceling out the Heisenberg interaction. Due to the multiplet structure of the excited levels, an anisotropic interaction appears [50] that can be bond dependent due to the various ways the octahedra can share an edge [48, 49]. It was then shown a year later that when considering the honeycomb iridates A_2IrO_3, one can also include the overlap of the d-orbitals, a Heisenberg interaction also appears [51]. Therefore, the most general Hamiltonian that represents these systems is one that includes both the Kitaev and Heisenberg interaction. A spin liquid phase has been shown to exist near the Kitaev point ($K = 1$) for $J < 1$ and several magnetically ordered phases are possible as well [52, 53]. However, at sufficiently low temperatures, some unexpected magnetic order not expected by the Heisenberg Kitaev (HK) model appears in Na_2IrO_3, a strong candidate that could host the Kitaev spin liquid as a ground state [49]. Efforts were made to explain that this phase could be part of the HK model if in the original derivation of the model one included next nearest neighbor interactions between various atoms in the honeycomb planes [54].

Some efforts were then focused on determining if the HK model was actually sufficiently general in describing honeycomb iridates that could host a Kitaev spin liquid. General symmetry constraints on edge shared octahedra show that another additional interaction is allowed, an anisotropic symmetric off-diagonal exchange of different spin components, $S^\alpha S^\beta + S^\beta S^\alpha$ [55]. The coupling is parameterized by Γ and is sometimes referred to as the Gamma interaction. Due to its coupling of different spin components, transformations on models containing the Gamma interactions are far and few between lending it naturally to numerical studies. It was then shown that a minimal model describing the honeycomb iridates would be given by [56]

$$J\sum_{\langle ij\rangle}\mathbf{S_i}\cdot\mathbf{S_j}+K\sum_{\langle ij\rangle_\gamma}S_i^\gamma S_j^\gamma+\Gamma\sum_{\langle ij\rangle_\gamma}(S_i^\alpha S_j^\beta+S_i^\beta S_j^\alpha)+\Gamma'\sum_{\langle ij\rangle_\gamma}(S_i^\alpha S_j^\gamma+S_i^\gamma S_j^\alpha+S_i^\beta S_j^\gamma+S_i^\gamma S_j^\beta). \tag{3.5}$$

The sums with the γ subscript take values of $\gamma = x, y, z$ leaving $\alpha \neq \beta$ to be the remaining spin components. The last interaction, the Gamma prime interaction (sometimes referred to as Γ_2 in which case $\Gamma = \Gamma_1$) stems from trigonal distortion, but is not always considered due to its lowering of the overall symmetry making it hard to

analyze. Understanding the phase diagram of 3.5 is extremely non-trivial and therefore only sections of the total J-K-Γ-Γ' parameter space are studied eventhough all interactions are possibly present by symmetry. On a 24 site cluster, a model containing the Heisenberg, Kitaev, and Gamma (HKG) interaction showed via exact diagonalization 4 magnetically ordered phases and the two exactly solvable Kitaev points ($K = 1, -1$) even when $\Gamma \neq 0$ which rendered more credence to the minimal model [55].

Other candidate materials outside of the honeycomb iridates are possible, with α-$RuCl_3$ being the main one. It was first shown that it has strong enough spin orbit coupling and weakly coupled honeycomb planes that make it amenable to 2D studies [57–59]. Crucially, it has Kitaev interactions and the Gamma interaction which are both comparable in magnitude [60]. There also appears to strong frustration above the magnetic ordering temperature believed to be due to the anisotropic nature of the Kitaev and Gamma interactions [59,61]. A study found that α-$RuCl_3$ in a magnetic field show a 2D thermal Hall conductance [62] in a field induced spin liquid phase. This is remarkably a fact predicted by Kitaev himself in his original study, namely that that the ground state of the gapped phase under a magnetic field can acquire edge modes due to having a non zero Chern number [41].

Understanding the phases that appear in models involving all three interactions are not only computationally demanding but also highly non trivial. The phase diagrams involve many different phases and the choices of order parameter become very important as well. Therefore, studying simplified systems involving at most two interactions at a time has been the common strategy when seeking to understand the phases.

3.3 Ladder Systems

A large portion of the studies conducted on honeycomb systems are done via exact diagonalization on small clusters with open boundary conditions. While yielding good results, the method is inherently limited to studying a handful of sites and cannot truly reproduce the thermodynamic limit. As the Kitaev spin liquid is to be hosted in 2D, the numerical techniques used must be able to appropriately probe larger system sizes. One idea is to use a quasi 2D strip of the honeycomb lattice and form a ladder of some length L with a number of sites $N = 2L$. While not entirely 2D, the ladder is amenable to use by DMRG as the system can easily be mapped to a chain with next nearest neighbor interactions (a figure is shown in the next section). Moreover, one

could either add more legs to the ladder, making it closer to a truly 2D system at the cost of longer range interactions in 1D. It is also possible to study a single leg of these ladders, which are just chains, as they are often easy to access numerically.

3.4 Kitaev-Gamma Chain and Ladder

While initially the HK model was studied, swapping in the Gamma interaction instead of a Heisenberg one yields the Kitaev-Gamma (KG) model. This was first done on a chain of of sites with alternating Kitaev bonds $K(S_i^\gamma S_{i+1}^\gamma)$ and Gamma bonds $\Gamma(S_i^\alpha S_{i+1}^\beta + S_i^\beta S_{i+1}^\alpha)$ where $\gamma = x, y$ and $\alpha \neq \beta$ are the remaining spin components [63, 64]. It can be shown that under a rotation about z of the spins by π, we must have that $(K, \Gamma) \equiv (K, -\Gamma)$, and hence part of the phase diagram must be symmetric (Namely about $K = 0$). It was also shown that there is a 6 site sub-lattice transformation that changes the Hamiltonian

$$H = \sum_{\langle ij \rangle_\gamma} K(S_i^\gamma S_j^\gamma) + \Gamma(S_i^\alpha S_j^\beta + S_i^\beta S_j^\alpha) \rightarrow H' = \sum_{\langle ij \rangle_\gamma} -K(S_i^\gamma S_j^\gamma) - \Gamma(S_i^\alpha S_j^\alpha + S_i^\beta S_j^\beta) \quad (3.6)$$

where $\langle ij \rangle_\gamma$ means that sites i, j lie on a $\gamma = x, y$ bond. Under this transformation, the Hamiltonian H' is much simpler and shows SU(2) symmetry when $K = \Gamma$. Note that this transformation is only possible when both the Kitaev and Heisenberg terms are present. Among the phases admitted, there is a "Kitaev" phase, near the $K \approx 1, \Gamma \neq 0$, which was not fully understood initially and the role of the Γ term was not understood. The same system was studied on a ladder geometry, where two KG chains were coupled by a z bond across each rung in the presence of a magnetic field [65]. A phase of interest is near the $K = 0, \Gamma = 1$ point, called the AF-Γ phase, has previously been studied and is believed to be a gapped spin liquid phase in the zero field limit [66]. The point $\Gamma = -1$, referred to as the FM-Γ point is understood via the 6 site sub-lattice transformation that is still valid in the ladder. When $K = \Gamma$, the KG ladder becomes the Heisenberg (anti)ferromagnetic ladder with a hidden SU(2) symmetry. In [65], it was shown that the $\Gamma = -1$ point is within the same phase as the point at which the KG ladder is equivalent to the antiferromagnetic Heisenberg ladder (HAFL). As the ground state of the HAFL is gapped, disordered and composed of singlets across the rung [67, 68], it was shown that the FM-Γ phase is therefore a rung singlet with hidden SU(2) symmetry. Several other phases are hosted in the KG ladder, with some spin liquid candidates among them. Overall, the importance of the Gamma interaction is still unknown, but when it is present the number of phases is substantial.

3.5 Heisenberg Gamma Ladder

The models previously mentioned all contain the Kitaev interaction since the overarching goal is to find a suitable theoretical model that includes interactions present in real materials that could host a Kitaev spin liquid. With some new found importance on α-$RuCl_3$ and the presence of the Γ term, it is possible to study these minimal models in the absence of the Kitaev term. In particular as mentioned above, the Heisenberg interaction is an important interaction in the relevant materials, particularly in the case of α-$RuCl_3$, and its behaviour when paired with the Gamma interaction warrants a study of its own.

A study has been conducted on a $N = 24$ site cluster in the honeycomb geometry with varied anisotropy of the Heisenberg and Gamma interactions [69]. Up to 10 magnetically ordered phases were found, with various ferromagnetic and antiferromagnetic, spiral, stripy, and dimerized states. The study points out that the AF-Γ spin liquid is unstable to anisotropy and unrelated to the Kitaev spin liquid in direct opposition to other studies that propose [70, 71]. These studies suggested that anisotropy could adiabatically connect the Kitaev spin liquid to the AF-Γ phase, however [69] claimed that no transition from an initial dimer phase is observed when passing through the $\Gamma = 1$ point. However, the study could not scale the cluster size and therefore not infer more about the phases in the thermodynamic limit.

There is no consensus just yet on the exact nature of the AF-Γ phase, but there is strong evidence to suggest that is may well be an SPT phase [72]. It remains unclear what exactly the nature of the Gamma interaction is (other than introducing frustration) and its behaviour in the presence of the Kitaev and Heisenberg interactions. Moreover, the 6 site sub-lattice transformation used in the KG model is spoiled by the Heisenberg term. To this end, this remainder of this work will numerically examine the Heisenberg Gamma model in the ladder geometry in order to access larger systems sizes using DMRG.

Chapter 4

Results

In this section we outline the main results in the analysis of the Heisenberg-Gamma ladder. We first introduce the model and the main methods used to classify phases and study the phase diagram. Then we give an overview of the phase diagram, its key features and a summary of all the phases. We separate the magnetically ordered phases into ferromagnetically and antiferromagnetically ordered states and and discuss their key features. We then discuss 3 potential SPT phases that show high entanglement and no obvious magnetic ordering.

4.1 The Heisenberg Gamma Ladder

Studying systems on honeycombs lattices can be difficult as the full 2D Hamiltonians are quite difficult to solve in the presence of anisotropy. To this end, we section a small strip of the honeycomb material and create a two leg ladder, ensuring that the bonds that are cut perpendicular to the length of the ladder are paired together in order to emulate periodic boundary conditions in the perpendicular direction (Fig. 4.1). The first interaction involved in this ladder geometry is the nearest neighbor Heisenberg interaction, which has been extensively studied in this geometry before. The second interaction is the Γ interaction, an anisotropic symmetric exchange interaction. The corresponding Hamiltonian is

$$H = \sum_{\langle i,j \rangle} J\mathbf{S}_i \cdot \mathbf{S}_j \; + \sum_{\langle i,j \rangle_\gamma} \Gamma(S_i^\alpha S_j^\beta + S_i^\beta S_j^\alpha), \tag{4.1}$$

where $\langle i,j \rangle_\gamma$ denotes the nearest neighbor bond of type γ. The possible kinds of bonds are $\gamma = x, y, z$ labeling the possible values of (α, β) as (y, z), (x, z), and (x, y) respec-

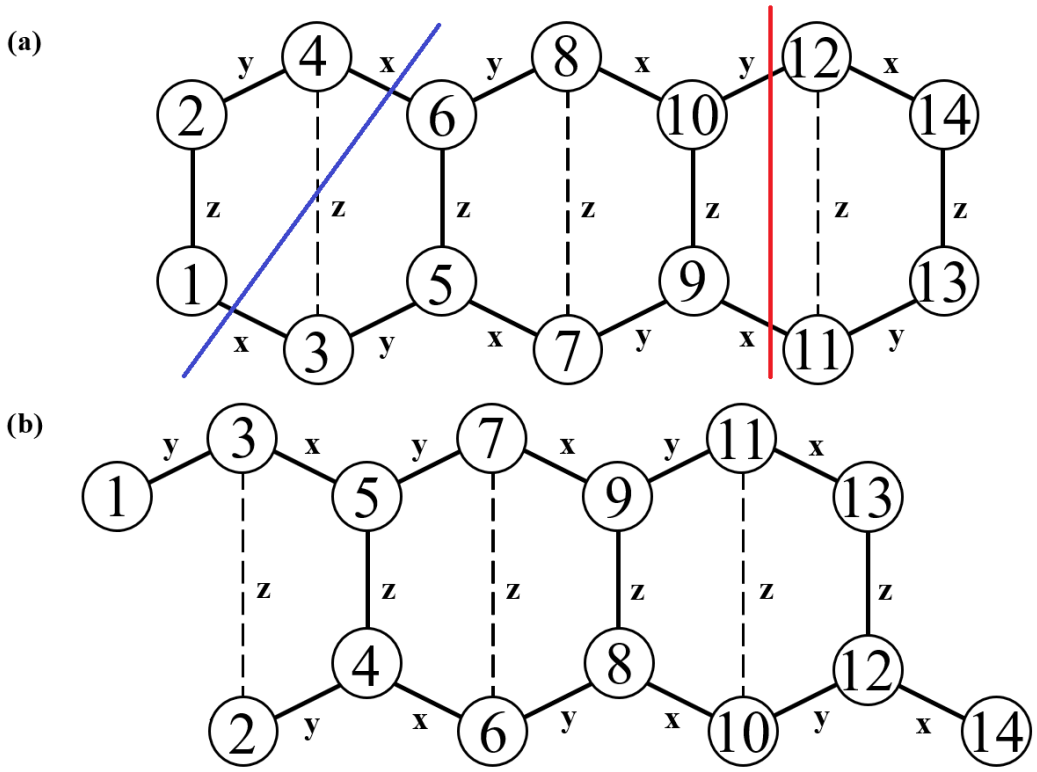

Figure 4.1: The two clusters of two leg J-Γ ladder with alternating x and y bonds across the legs which are connected by the z bonds along the rungs. The dashed lines indicate that the z bonds are paired together. (a) Cluster A formed from a regular ladder comprised of 3 unit cells where the red line indicates the bond cut and the blue line indicates the rung cut. (b) Cluster B formed from cutting the rungs from cluster.

tively. In other words, γ labels the missing spin component exchange present in $S_i^\alpha S_j^\beta$. The J-Γ ladder comprises alternating x and y bonds along the both legs, connected by z bonds along the rungs. The unit cell of the ladder is comprised of 6 sites, in Fig. 4.1 a three unit cell ladder is shown as a strip of a honeycomb lattice. We will also use a second cluster of sites referred to as the rung cut cluster, named after the fact that it is made from the ladder with diagonal cuts along the ladder. In this study we will refer to the first cluster as A and the second rung cut cluster as B. The Heisenberg and Γ couplings are parameterized by

$$J = \sin(\phi),\ \Gamma = \cos(\phi), \tag{4.2}$$

Table 4.1: Summary of the main features of all of phases of the J-Γ ladder. The phase symbol and the critical values of ϕ/π for which the phase exists are listed as well as the magnetic ordering. The last column indicates the presence of a energy gap in the spectrum in the thermodynamic limit

Phase	ϕ_c / π	Magnetic Ordering	Energy Gap
AF-Γ	-0.017 - 0.025	None	Yes
δ	0.025 - 0.077693	None	Possibly Gapless
AF	0.077693 - 0.380	AFM	Yes
RS	0.380 - 0.790	RS	Yes
AF-Z	0.790 - 0.840	AFM-Z	Yes
FM-Γ	0.840 - 1.108	None	Yes
FM	1.108 - 1.500	FM	Yes
FM-Z	1.500 - 1.775	FM-Z	Yes
Υ	1.775 - 1.820	None	Yes
Ω	1.820 - 1.840	None	Yes
FM-XY	1.840 - 1.983	FM-XY	Yes

which adiabatically connects the Heisenberg and Γ ladder in both antiferromagnetic and ferromagnetic regimes. Several values of phi are well known: $\phi = 0, \pi$ are the antiferromagnetic and ferromagnetic Γ ladder which have been studied numerically previously [67, 68]. For $\phi = \pi/2, 3\pi/2$, the antiferromagnetic Heisenberg ladder, known to be a in a gapped rung singlet phase, and the ferromagnetic Heisenberg ladder have and continue to be studied analytically and numerically. Spin ladders can also host symmetry protected topological (SPT) phases for which symmetries forbid the wavefunction of the system to be adiabatically related to a product state unless the symmetries are broken. Moreover, the degeneracy of the ground state in an SPT phase is dependent upon the boundary conditions. In open boundary conditions, states in the ground state manifold can exhibit edge modes while in periodic boundary conditions the state is gapped with a unique ground state. In the case of a ladder geometry, there are only two unique open clusters possible due to its one dimensional nature: the normal ladder (cluster A) and the rung cut (cluster B). We will specify the choice of OBC conditions used as different SPT phases may show edge modes for only one kind of open geometry and not the other.

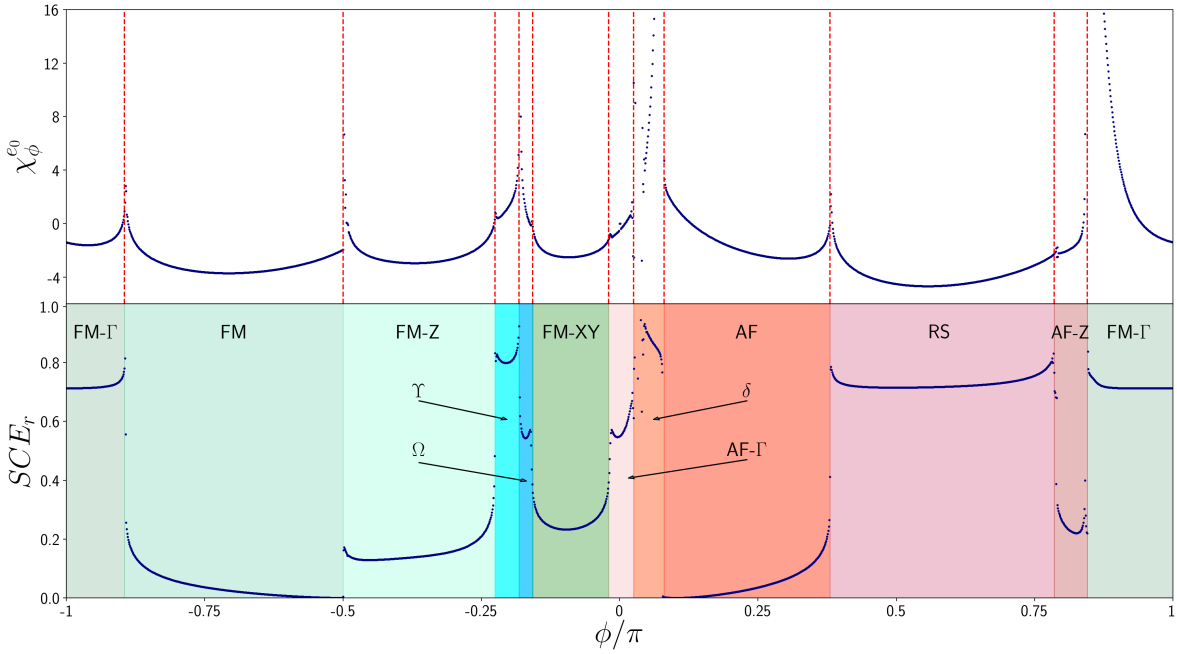

Figure 4.2: Phase diagram of the J-Γ ladder as function of ϕ/π from iDMRG with a unit cell of N=24 and a resolution $\Delta\phi/\pi = 1.0 \times 10^{-3}$. Top Panel is the second derivative of the ground state energy per site with respect to ϕ with the identified critical values of ϕ identified with the red vertical lines. Bottom panel is the logarithm of the 1st eigenvalue of the reduced density matrix across bond $N/2 - 1$.

4.2 Methods

The main tool used in this analysis is the finite density matrix renormalization group (DMRG) and its infinite sized version, the infinite density matrix renormalization group (iDMRG). The finite sized version will be used to obtain the ground state and the next 4 excited states with open boundary conditions (OBC) and periodic boundary conditions (PBC). In the OBC scheme, we have a maximal bond dimension $\chi = 1000$ and a precision of $\epsilon = 10^{-13}$, while in the PBC scheme we have $\chi = 1200$ and $\epsilon = 10^{-11}$. To obtain the ground state in the thermodynamic limit, produce the phase diagram, and calculate the bulk correlation functions, we use iDMRG with $\chi = 1000$ and $\epsilon = 10^{-11}$. In order to ensure that we detect all possible phases, we use a small resolution of $\Delta\phi/\pi = 0.001$. To detect the phases and their transitions, we use two measures of the ground state wavefunction, the first being the susceptibility of the ground state energy per spin with respect to ϕ

$$\chi^e_\phi = -\frac{\partial^2 e_0}{\partial \phi^2}. \tag{4.3}$$

While χ^e_ϕ is straightforward to calculate, it is not always easy to notice a quantum phase transition using χ^e_ϕ as it depends strongly on the resolution $\Delta\phi$ chosen and on the convergence of the wavefunction. Instead of probing the energy, it is possible to probe the structure of the many body state itself via its bipartite entanglement properties. We can cut the ladder across a bond n in the ladder and form the reduced density matrix ρ_n. The eigenvalues λ_i of ρ_n provide the bipartite von Neumann entropy S_n across bond n, which is sometimes referred to as the entanglement entropy (EE). The eigenvalues change slowly away from a quantum critical point but rapidly near one [73]. We therefore choose to track part of the first term in the EE

$$SCE = -\ln(\lambda_1), \tag{4.4}$$

in our system which is referred to as the single copy entanglement in the context of quantum information [74]. When the ground state is in a product state, we must have that $\lambda_1 = 1$ and $\lambda_n = 0$, $\forall n > 1$ implying that $SCE = 0$. On the other hand, if our system is not in a product state, $\lambda_1 < 1$, and hence $SCE > 0$. In the ladder geometry, the only two unique bipartitions are made either cutting through two leg bonds or through two leg bonds and a rung shown in Fig. 4.1. We will refer to the odd numbered bond cut as rung cut, and the even numbered bond cut as a bond cut as the former cuts through a rung and two leg bonds while the latter cuts only through

two leg bonds. While either partition can be used for our purposes, we have found that SCE is larger across rungs cuts making it clearer to see the phase transitions compared to the bond cuts. We therefore adopt the convention that SCE refer to the single copy entanglement formed across such rung cuts if not direct denote it with a subscript r . In order to characterize the magnetic ordering of the phases, the spin correlation functions $\langle S_i^\alpha S_{i+n}^\alpha \rangle$ as well as the on-site magnetization $\langle S_i^\alpha \rangle$. To detect magnetic ordering that is not seen through the correlation functions, we use the scalar chirality. For a spin at site i we denote $\mathbf{S_i} = \sigma_\mathbf{i}/2$ and define the scalar chirality as

$$\kappa = \langle \sigma_i \cdot (\sigma_{i+1} \times \sigma_{i+2}) \rangle. \tag{4.5}$$

This indicates the presence of chiral ordering and incommensurability with the lattice. Furthermore, when referring to a phase we take a single point in the phase diagram as a representative member. These points are chosen such that they have the largest gap within their phase to ensure that DMRG can efficiently calculate the ground state. Since the entanglement is inversely related to the gap [6], the representative members were taken to be in the center of each phase in Fig. 4.2 where SCE is constant and the smallest. Due to a large portion of the phases of interest being centered around $\phi = 0$, in Fig. 4.2 ϕ is in the interval $(-\pi, \pi)$ rather than the values of $(0, 2\pi)$ present in Table 4.1.

4.3 Magnetically Ordered Phase

Here we present and discuss the magnetically ordered phase as classified through their spin spin correlation functions. The two main categories are phase that show ferromagnetic and antiferromagnetic ordering. The rung singlet, AF-Γ, and FM-Γ phases are not exactly magnetically ordered and will be discussed in more detail.

4.3.1 AF Phases

There are four phases identified as antiferromagnetic (AF), either by being adiabatically connected to known points or have clear magnetic ordering. In Fig. 4.4 the spin correlations can be seen for each phase.

AF-Γ

Starting from the smallest values of ϕ, the AF-Γ phase is shown in figure 2 panel (a). At $\phi = 0$, $J = 0$ and $\Gamma = 1$, i.e. only the Γ interaction is present and positive, hence

the name *antiferromagnetic* Γ (AF-Γ) phase. It has already been studied in the context of the Kitaev Gamma ladder in the presence of a field and is already known (REF).

AF

For $\phi \in (0.075, 0.38)$, we have the AF phase, named after the fact that all of its spin correlation functions show clear long range antiferromagnetic ordering of equal magnitude for each spin component.

Rung Singlet

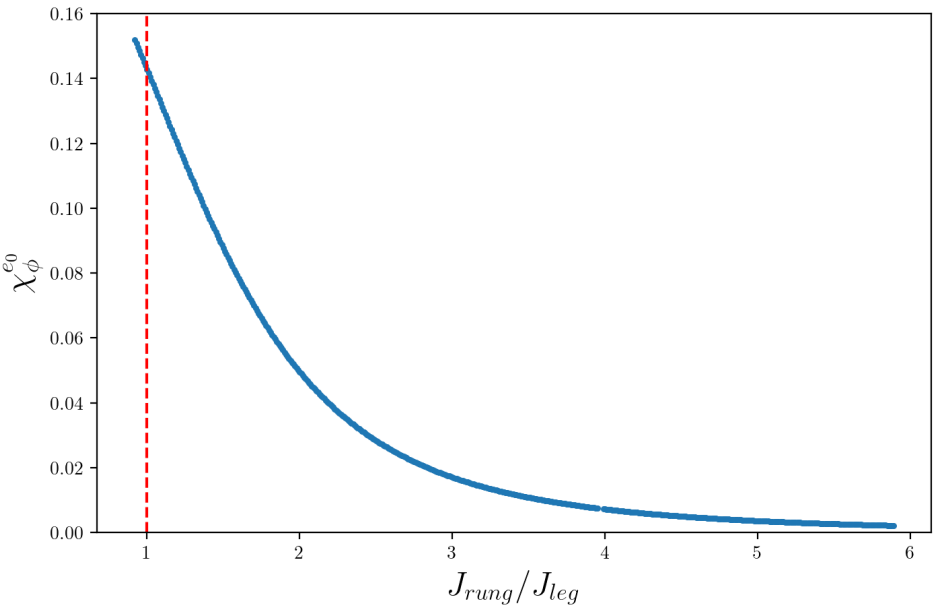

Figure 4.3: Susceptibility of the ground state energy $\chi_\phi^{e_0}$ as the ration of J along the rungs of the ladder J_{rung} and the legs J_{leg} is tuned. This was done in iDMRG by increasing the ratio $\Delta(\frac{J_{rung}}{J_{leg}})$ by 0.01 for $\phi = 0.6\pi$.

Directly after, for $\phi \in (0.38, 0.79)$, there is the rung singlet (RS) phase containing the point where $J = 1, \Gamma = 0$, also known as the antiferromagnetic Heisenberg ladder. Its ground state is known to be in a disordered ground rung singlet phase (insert reference), where across each rung the sites are coupled into a spin singlet. While the spin correlations shown in Fig 4.4 do not show disordered behavior, the ground state that we obtained can be connected adiabatically to a pure rung singlet state. The Heisenberg coupling, J, can be separated into two couplings, J_{leg} and J_{rung}, one

coupling across the legs and one across the rungs. By increasing the ratio of J_{rung}/J_{leg}, we approach the limit of rung singlets forming across the rungs. After obtaining the ground state energies while increasing the coupling ratio, the susceptibility χ^e_ϕ shows no divergences, hence the initial phase and the RS phase must be one in the same. The results can be seen in Fig 4.3, where the red line indicates the state in the $J\Gamma$ ladder with a ratio of 1. As the ratio is increased and singlets become more favorable, no divergence in $\chi^{e_0}_\phi$ is observed.

AF-Z

Lastly, for $\phi \in (0.79, 0.84)$, the spin correlations look similar to those of the AF phase, except that the magnitudes are not all the same. Since the $S^z_1 S^z_n$ correlations are larger than the $S^x_1 S^x_n$ and $S^y_1 S^y_n$ correlations, which are equal, we call this the AF-Z phase.

4.3.2 FM Phases

Similar to the AF phases, we have four phases identified via known points and their correlations functions. Fig. 4.5 shows their spin correlation functions.

FM-Γ

Due to containing the point $J = 0, G = -1$, the phase for the points $\phi \in (0.84, 1.11)$ are said to be in the *ferromagnetic* Γ (FM-Γ) phase. Just like its antiferromagnetic counter part, it has already been studied before and will be discussed in section 4.4.

FM

For $\phi \in (1.11, 1.5)$, we have a long range ordered phase in which each spin correlation function is of equal magnitude, which we name the ferromagnetic (FM) phase.

FM-Z

Neighboring it is the FM-Z phase for $\phi \in (1.5, 1.775)$, which looks slightly similar to the FM phase but is such that the $S^z_1 S^z_n$ correlations are larger than the $S^x_1 S^x_n$ and $S^y_1 S^y_n$, which are equal.

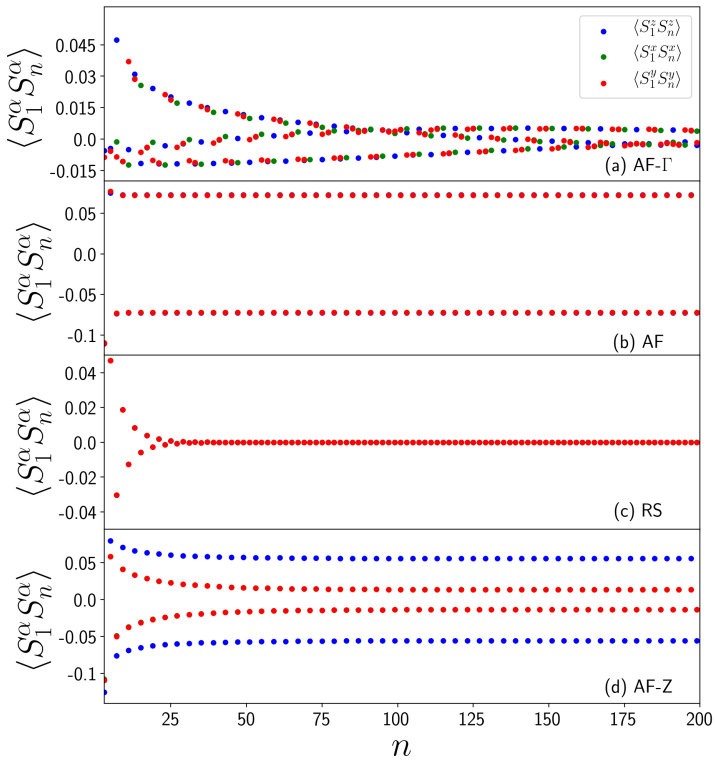

Figure 4.4: Spin correlation functions $\langle S_1^\alpha S_{1+n}^\alpha \rangle$ of the rung singlet phase and the antiferromagnetic ones obtained from iDMRG along the lower leg (odd numbered sites) of the ladder starting at $n = 3$ and ending at $n = 199$. Each panel shows a representative member of the antiferromagnetic and rung-singlet phases chosen to show the clearest magnetic ordering. Panel (a), (b), (c) and (d) correspond to, respectively, $\phi = 0.064\pi, 0.249\pi, 0.499\pi, 0.799\pi$ which are the AF-Γ, AF, RS, and AF-Z phases.

FM-XY

Lastly, there is the FM-XY phase for $\phi \in (1.84, 1.98)$. Depending on which leg of the ladder is analyzed, the spin correlations have either the $S_1^x S_n^x$ or $S_1^y S_n^y$ correlation marginally larger than the other at small n and then finally equalling each other at larger n. Along both legs, the $S_1^z S_n^z$ correlations are smaller than the other two and non-zero. In figure 2, the FM-XY phase in panel (d) shows that $S_1^y S_n^y$ is slightly larger along leg 1, and hence across leg 2, $S_1^x S_n^x$ is slightly larger, but along both legs $S_1^z S_n^z$ is still the smallest.

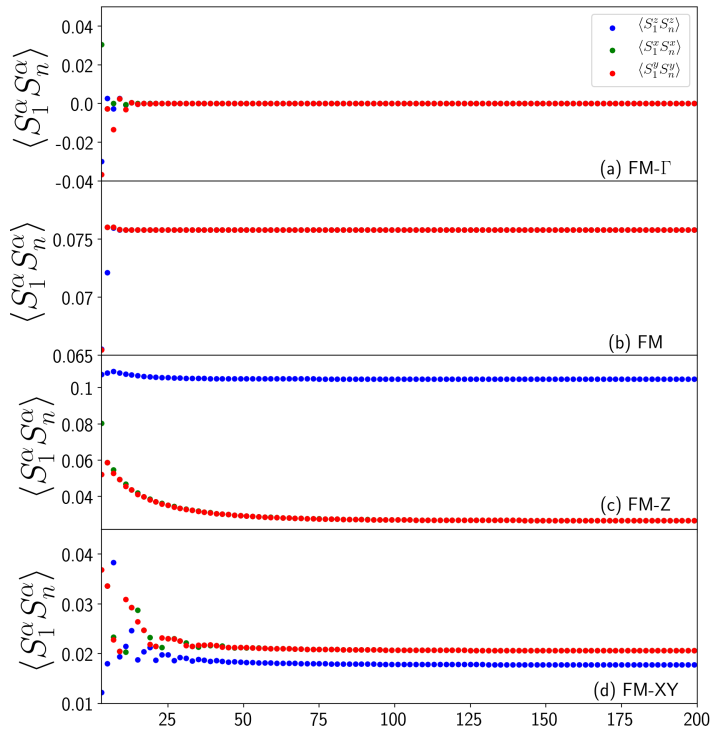

Figure 4.5: Spin correlation functions $\langle S_1^\alpha S_{1+n}^\alpha \rangle$ of the ferromagnetic phases obtained from iDMRG along the lower leg (odd numbered sites) of the ladder starting at $n = 3$ and ending at $n = 199$. Each panel shows a representative member of the ferromagnetic phases chosen to show the clearest magnetic ordering. Panel (a), (b), (c) and (d) correspond to, respectively, $\phi = 0.899\pi, 1.299\pi, 1.649\pi, 1.849\pi$ which are the FM-Γ, FM, FM-Z, and the FM-XY phases.

4.4 The AF-Γ and FM-Γ Phases

The points on the phase diagram in Fig 4.2 where $\phi = 0, \pi$, the AF-Γ and FM-Γ phases respectively, have previously been studied when paired with the Kitaev interaction in the chain and ladder geometries. It was shown that the AF-Γ point is adiabatically connected to an SPT phase and thus the phase from $\phi \in [0, 0.025\pi)$ in the J-Γ ladder must be this SPT phase by universality. Similarly, in the Kitaev-Γ ladder, the FM-Γ ladder was shown to be connected to a rung singlet phase (RS) with a hidden U_6 local order. This is due to the fact the Kitaev-Γ ladder can be transformed to Heisenberg-like ladder of opposite sign. When the Kitaev and Γ interactions are of equal magnitude and sign, the ferromagnetic and antiferromagnetic Heisenberg ladders appear. The antiferromagnetic ladder appears when both interactions are negative and this phase extends

to the case where only the Γ is non zero and negative while the Kitaev interaction is absent. Therefore, the phase from $\phi \in [0.84\pi, -0.89\pi]$, where $\Gamma = -1, J = 0$ must, by universality, be the antiferromagnetic Heisenberg ladder, known to be in a gapped RS phase, with a hidden U_6 symmetry.

4.5 Potential SPT phases

Out of the 11 phases we have identified, 3 possibly new SPT phases, the δ,Υ, and Ω phases which all show no magnetic ordering in the thermodynamic limit with large entanglement across the rung cut of the ladder. All three phases show no scalar or vector chirality as well, and therefore show no long range magnetic order. The spin correlations are shown in figure 4.6. The first indication is that the reduced density

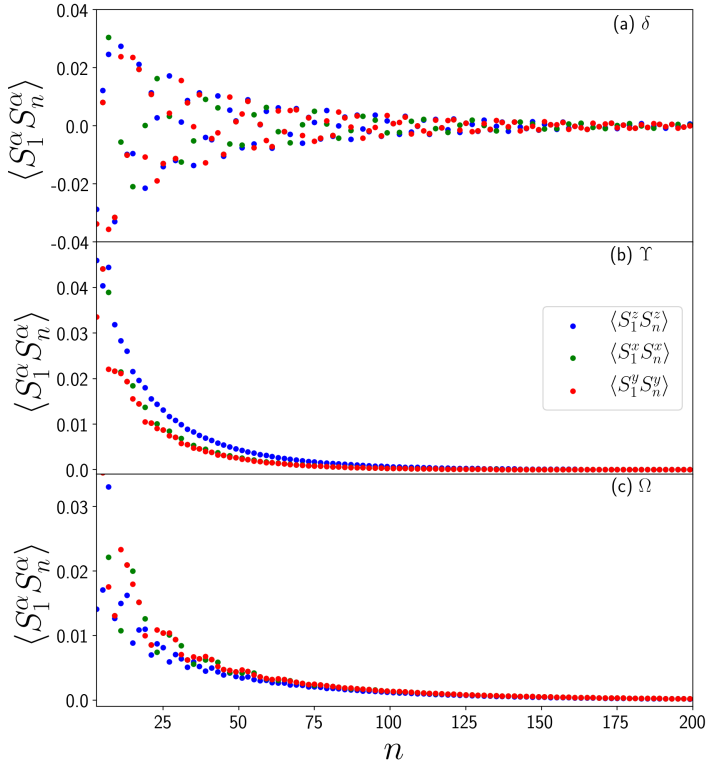

Figure 4.6: Spin correlation functions, $\langle S_1^\alpha S_{1+n}^\alpha \rangle$ of the potential SPT phases versus n at $\phi = 0.064\pi, 1.799\pi, 1.829\pi$ obtained from iDMRG. The calculations are performed along the first leg of the ladder, starting at $n = 3$ and ending at $n = 199$.

matrices formed across the rung cuts ρ_r and the bond cuts ρ_b have an exact doubling in the thermodynamic limit. The δ and Υ phases have a doubling of the eigenvalues

across the rungs cuts while the Ω phase has a doubling across the bond cuts. Using finite DMRG we have also determined that all three of the phases are gapped when periodic boundary conditions are imposed. Fig 4.7 shows the spin gap $\Delta E = E_1 - E_0$ between the first excited state and the ground state as N is increased. As gapless states are only truly gapless in the thermodynamic limit, $\Delta E \propto 1/N$, increasing N should either yield a gap tending toward zero linearly in $1/N$ or approaching a constant value. Fig 4.7 shows that all three phases are indeed approaching some constant limit. Another way to verify this is too examine the correlation length within each of the phases as $\xi \propto 1/\Delta E$ [16]. Moreover, the entanglement S is proportional to the correlation length in 1D spin systems [75] which means that $S \propto 1/\Delta E$. Since we are tracking the SCE across the transitions and that the SCE is part of the total entanglement S, we must have that the gap is largest where the SCE is the smallest within each phase. Therefore, picking a representative point for each phase where the SCE is the smallest gives the largest gap and is the most stable. Upon constructing the transfer matrix in iDMRG, the correlation lengths are extracted to be $\xi_\delta \approx 46.66$, $\xi_\Upsilon \approx 26.06$, and $\xi_\Omega \approx 42.66$. These values agree with the relative ordering of the gaps of the phase, namely $\Delta_\delta < \Delta_\Omega < \Delta_\Upsilon$, from finite DMRG and so the phases are likely gapped. Under appropriate boundary conditions, all three phases should show edge modes in the form of non zero magnetization at the edges of the cluster. Due to this, the states also show degeneracy of the ground state, namely there are 4 low lying states that are close in energy in open boundary conditions, which is in contrast to the unique gapped ground state in periodic conditions. The edge modes present are very similar to one another and are thus difficult to distinguish. In order to differentiate between these degenerate states, we follow [76] and examine the total magnetization of the states in the ground state manifold. If the edge modes are to be truly localized at the edges of the clusters, there should little contribution from the bulk to the overall magnetization. As the clusters are made larger, the magnetization should become constant if the edge modes are the only sections of the ladder that support non zero magnetization. Therefore we construct the total magnetization $\tilde{S}^n = \sum_i S_i^n$ for axis n in the 4-fold degenerate ground state manifold. As the ladder is a section of a honeycomb lattice, we analyze axes $a = (1, 1, -2), b = (1, -1, 0)$, and $c = (1, 1, 1)$. Diagonalizing $\tilde{S}^n$ should yield an eigenvalue structure of $s, -s, 0, 0$ where three of the states are spin polarized states and one 0 state is singlet. This should detect what kind of pairing at the ends of the chain is present and therefore should provide a way for the 4 states to be distinguished. In Fig 4.5 the largest eigenvalue s of $\tilde{S}^n$ is shown for in plane axes a, b, and c as the system size N is increased. We see that the δ phase shows decaying eigenvalues while phases Υ

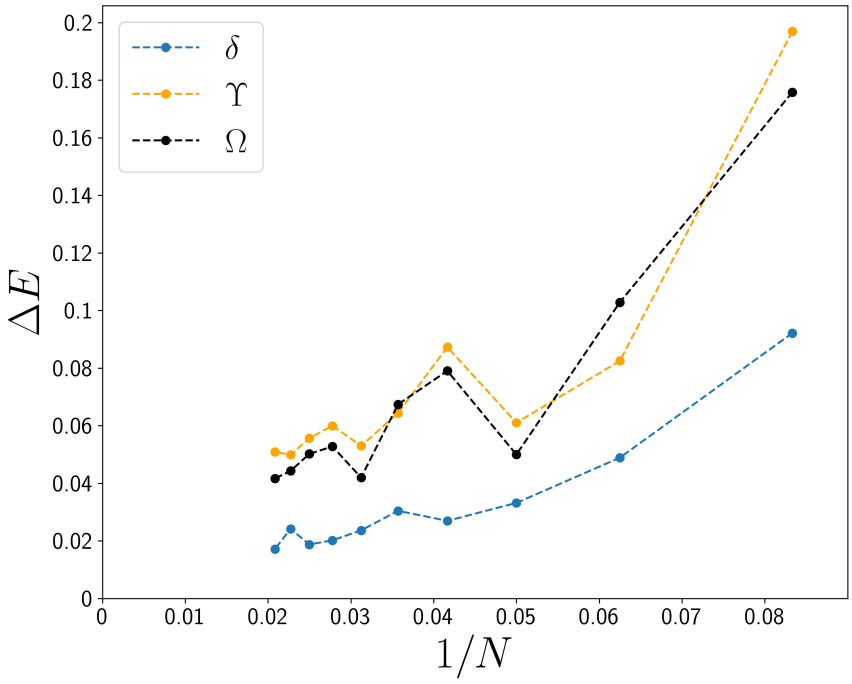

Figure 4.7: Energy gaps $\Delta E = E_1 - E_0$ of the δ,Υ, and Ω phases between the ground state and the first excited state obtained through finite DMRG with a maximal bond dimension $\chi = 1200$. The length of the ladder starts at $N = 12$ sites, incremented by 4 sites each time to maintain periodic boundary conditions, until a max of $N = 48$. The phases have small gaps with the magnitudes agreeing with the value of the correlation length obtained from the transfer matrix.

and Ω show increasing eigenvalues. However, the system sizes that are probed do not exceed one correlation length in the case of the δ and Υ phase.

4.5.1 The δ phase

While trying to perform the numerical analysis, the members of the δ phase show poor convergence as seen in the scattering of $\chi_\phi^{e_0}$ in Fig 4.2 near the AF-Γ to δ transition point. In the δ phase, the spin correlation functions all decay and show no scalar or vector chirality in this phase like the other three SPT phases. However, the correlation functions in Fig 4.6 show that it is possible to have an ordering that is incommensurate with that of the lattice. Namely, the decaying correlations in the δ phase show no pattern in the sign of the correlation functions. To this end, we examine the structure factor $S^{\alpha\alpha}(k) = \sum_{n=1}^{L} e^{ikn}\langle S_1^\alpha S_n^\alpha\rangle$ for L sites in the ladder. Since the transitions into

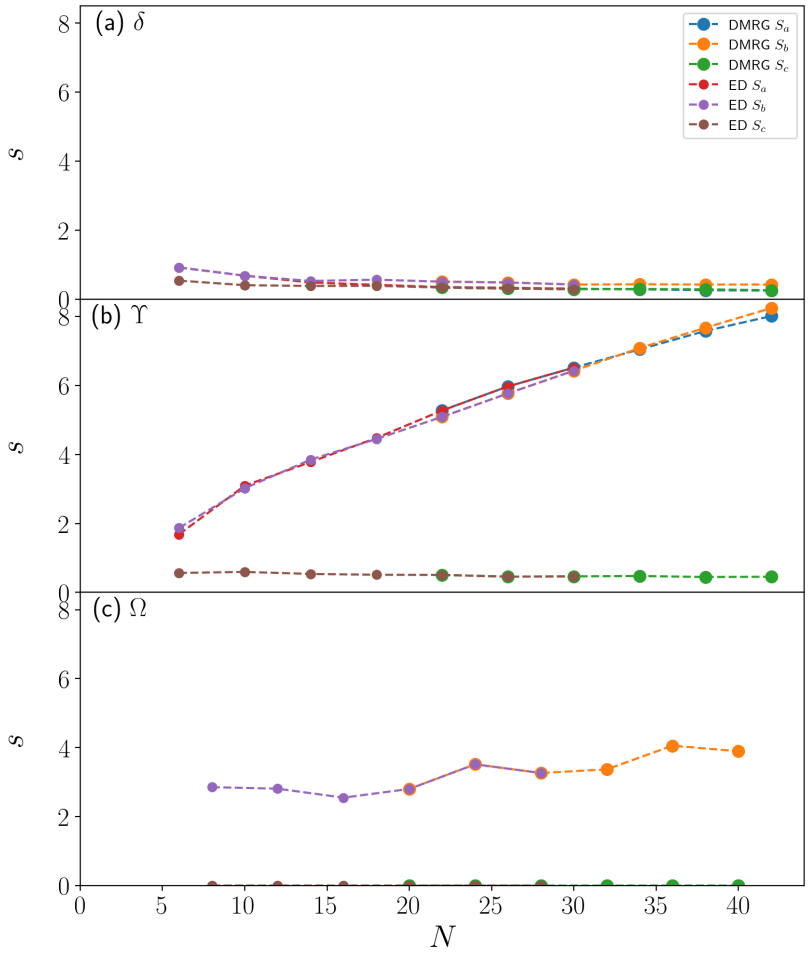

Figure 4.8: Leading eigenvalue $|s|$ of the total magnetization $\tilde{S}^n$ along axis n for the δ (top),Υ (middle), and Ω (bottom) as a function of cluster size N. The first sizes until N=28 are obtained with exact diagonalization (ED) while the remaining larger sizes are obtained with DMRG.

and out of the δ phase have convergence issues, we will examine the behaviour of the structure factor as we sweep through the AF-Γ phase to the AF phase. In Fig 4.9 the zz structure factor is shown starting in the pure AF-Γ phase at $\phi = 0$ in red. The wavevector k is initially set at $k \approx 2\pi/3$ with a small weight also surrounding $k = 0$. As ϕ increases, the weight at $k = 0$ begins to decrease as the $k \approx 2\pi/3$ peak begins to increase, both staying fixed at their wave vectors. Eventually the $k = 0$ peak will disappear entirely and only the larger $k = 2\pi/3$ one will remain. As the critical value $\phi = 0.025\pi$ is crossed, we enter the δ phase, denoted by the blue color, and the peak begins to move towards $k = \pi$ just before the transition to the AF phase in green.

Once we have crossed the critical value of $\phi = 0.077693\pi$, the wavevector is now firmly at $k = \pi$ which agrees with the fact that the AF phase has Néel order in the z direction. As the AF phase is a product state with antiferromagnetic order, $S^{zz}(k)$ should be centered around $k = \pi$ immediately, providing the +/- alternating spin pattern. It

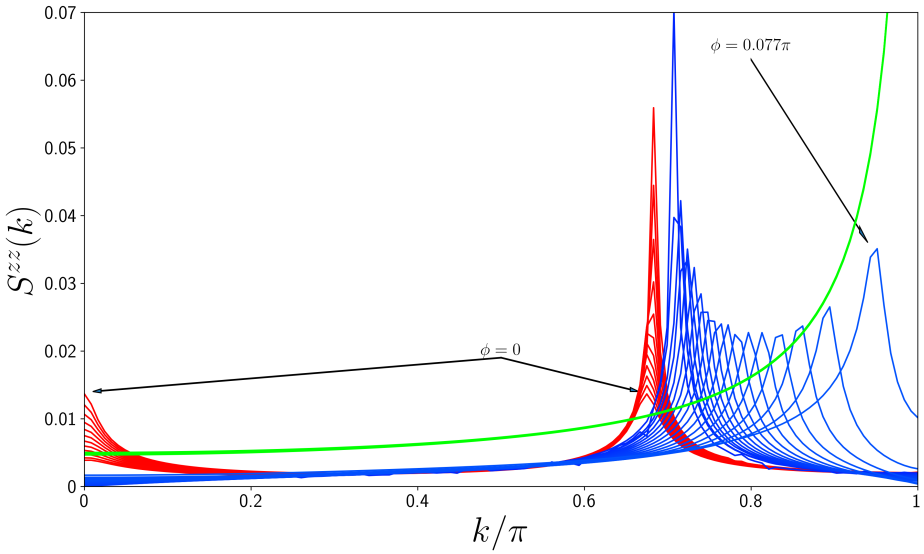

Figure 4.9: Structure factor $S^{zz}(k)$ from the $\langle S_i^z S_{i+1}^z \rangle$ correlation functions of the AF-Γ, δ and AF phases obtained from iDMRG along the first leg of the ladder. The red color indicates where $S^{zz}(k)$ is in the AF-Γ phase, transitioning to the δ phase in blue, and ending in the AF phase in green. $S^{zz}(k)$ at $\phi = 0$ is pointed out as having two peaks, one at $k = 0$ and at $k \approx 2/3$. The last point in the δ phase in this sweep is also pointed out at $\phi = 0.077\pi$ before the transition to the AF phase occurs.

is difficult to see the gradual change of $S^{zz}(k)$ across the transition point due to the precision in k space used initially in Fig 4.9. Once increased, one can see a smooth transition to the $k = \pi$ peak as shown in Fig 4.10. Near the transition point, the structure factor in the δ phase (in blue) moves towards the $k = \pi$ as the weight also increases. Once in the AF phase (in green), the k value is the same but the weight is significantly larger. It would seem that the peak is also broader in the AF phase, but this is only due to $S^{zz}(k)$ being so small in the δ phase, in the AF phase it is much larger in comparison with a maximal value of ≈ 0.8.

The δ phase shows continuous behaviour of the xx and yy structure factors when moving through the AF-Γ, δ, and AF phases. In Fig 4.11, $S^{xx}(k), S^{yy}(k), S^{zz}(k)$ are all plotted together for the three phases in question. In the first panel, there are 3 peaks

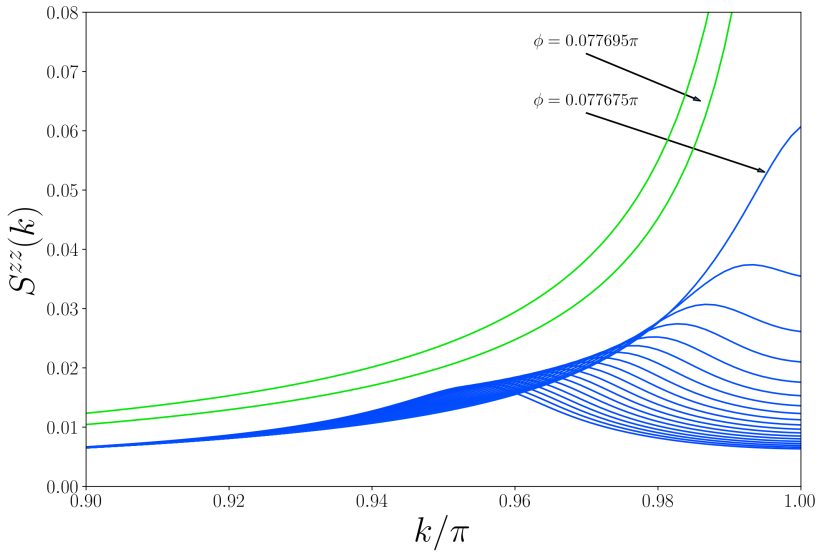

Figure 4.10: Structure factor $S^{zz}(k)$ from the $\langle S_i^z S_{i+1}^z \rangle$ correlation functions of the δ and AF phases obtained from iDMRG along the first leg of the ladder. Starting at $\phi = 0.077314\pi$ in the δ phase in blue, we sweep through to the AF phase at a maximum value of $\phi = 0.077716\pi$ in green. The last value in the δ phase occurs at $\phi = 0.077675\pi$ while the first value in the AF occurs at $\phi = 0.077695\pi$ which are both centered around $k = 1$.

visible in the AF-Γ phase for $\alpha = x, y$ at $k \approx 0, \pi/3, 2\pi/3$ while only two peaks are seen for $\alpha = z$ at $k = 0, 2\pi/3$. Once in the δ phase, the first peak at $k = 0$ is gone for all α and the remaining peaks initially situated at $k = \pi/3, 2\pi/3$ in the AF-Γ phase begin to move. For $\alpha = z$, the single peak begins to move towards $k = \pi$ as mentioned previously, while the two peaks for $\alpha = x, y$ begin to separate. The $k = \pi/3$ peak moves, throughout the δ phase, towards $k = 0$ and decays in value while the $k = 2\pi/3$ peak moves towards $k = \pi$ like in the $\alpha = z$ case. Finally, all of the structure factors are peaked at $k = \pi$ once in the AF phase. Therefore, $S^{\alpha\alpha}(k)$ in the δ phase is some continuous mixture of the AF-Γ structure factor and the AF structure factor.

The transition between the δ and the AF phase seen through the correlation length reveals a very sharp transition between the two phases. When crossing the $\phi = 0.077693\pi$ point, a very sudden divergence in the correlation length ξ appears as $\xi \propto 1/\Delta$ [16] and the gap Δ closes at a transition point [33]. In Figure 4.12 we see that there are two transitions as expected. The first transition between the AF-Γ and δ phases agrees with $\chi_\phi^{e_0}$ and ξ diverges at $\phi \approx 0.025\pi$. It must be noted that due to memory constraints,

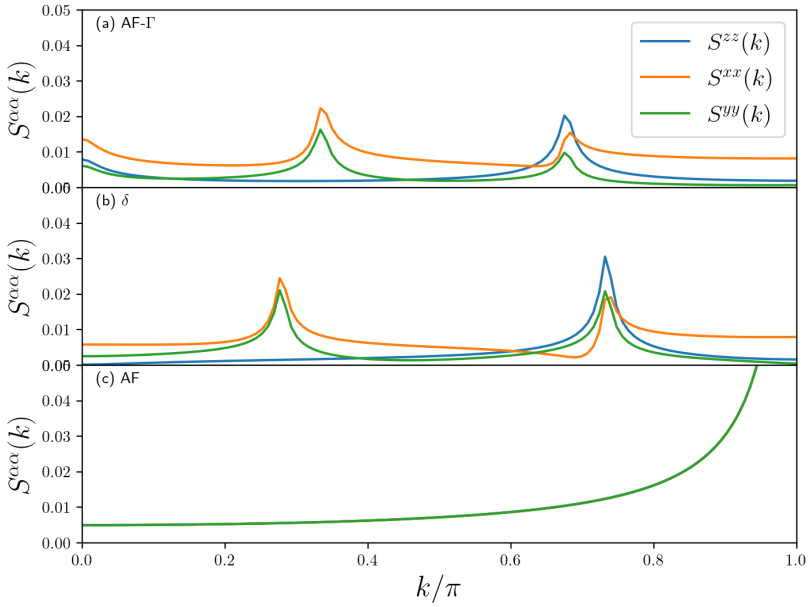

Figure 4.11: Structure factor $S^{\alpha\alpha}(k)$ for $\alpha = x, y, z$ obtained from iDMRG along the lower leg of the ladder. The representative points of the AF-Γ, δ, and AF phases are at $\phi = 0.009\pi, 0.054\pi, 0.090\pi$ respectively.

the maximum bond dimension used in the calculation of the correlation length is much smaller than that in the calculation of the phase diagram since the transfer matrix scales as χ^4. Within the δ phase, the correlation length is rather large until we begin to approach the second transition point at $\phi = 0.077693$. To the left of the transition point, the value of ξ is constant til a sharp transition occurs to the AF phase, where the correlation length is of order unity as expected. As χ is increased, ξ before the second transition point remains more or less constant indicating that the phase is probably gapped. If it were gapless, as χ is increased ξ would keep growing which is not the case here. Its still of note though that the gap is smaller than the other two potential SPT phase by a factor of 2. To right of the second transition point, $\xi = O(1)$ and therefore the AF must have a gap that is much larger than what is in the δ phase.

4.5.2 The ϒ Phase

Due to the growing eigenvalues of the magnetization across the a and b axes in the ϒ phase as shown in 4.5, it is likely that there is some magnetic ordering in the plane of

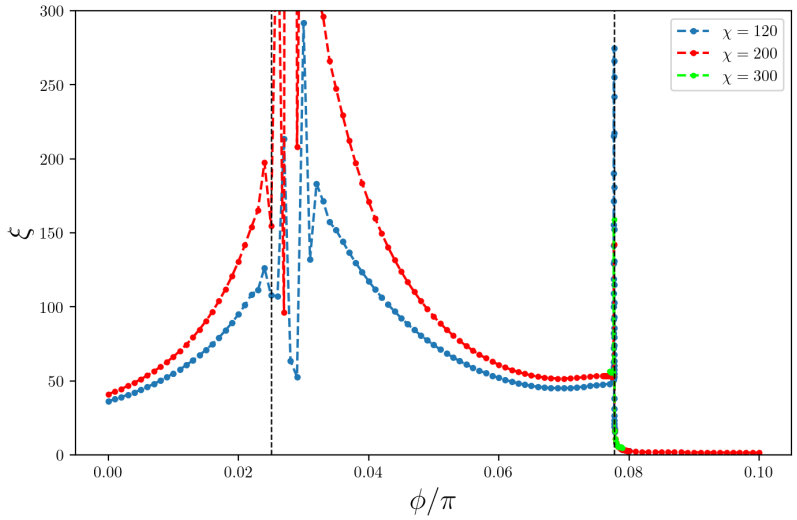

Figure 4.12: Correlation length ξ from the second eigenvalue of the transfer matrix from iDMRG with a bond dimension of 120, 200 and 300 plotted in blue, red and green respectively. The first black line denotes the transition from the AF-Γ inferred from the phase diagram (4.2) at $\phi = 0.025\pi$ and the second black line denotes the transition between the δ to AF transition at $\phi = 0.077693\pi$ which agrees with the $S^{zz}(k)$ data.

the ladder. If the phase were to truly be an SPT phase, edge modes would appear and remain stable as N is increased, while the bulk remains non magnetic. Moreover, as a magnetic field is introduced along the a or b axes, the magnetization should greatly increase along those axes while remaining unchanged in the bulk. One can directly plot the magnetization down the chain but not much information will be gained. Figure 4.13 shows the 4 states in the ground state manifold and their on-site magnetization along the length of the ladder. All 4 panels show some magnetization that persists longer into the ladder than what the correlation length ($\xi \approx 26.06$) would imply if the there were to edge modes. Moreover, as the states are assumed to be degenerate, is is difficult to obtain all of the states in the ground state manifold as DMRG works best when gaps between the energy levels are present. We can split the degeneracy by applying a small magnetic field in order to isolate the lowest energy state out of the 4 and analyze its properties. We apply the field along the b axis as we suspect that there is the possibility of ordering in the plane of the ladder. As shown in Figure 4.14, we fix $N = 30$ and turn on a negative magnetic field (its magnitude is plotted on the x-axis) and track the center site magnetization along the b direction in the ladder at $n = 15$. The magnetic field increases $\langle S^b_{15} \rangle$ linearly til $B = -0.001$ where the magnetization begins to level

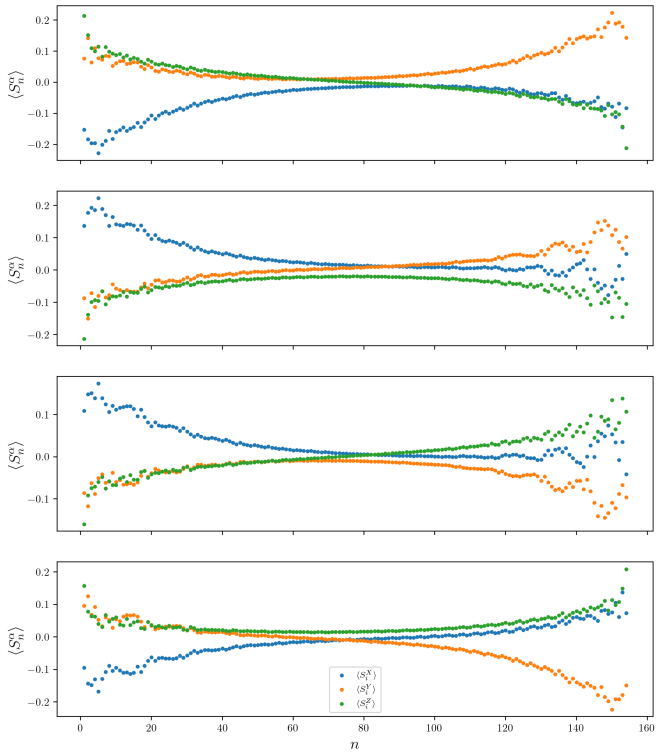

Figure 4.13: On site magnetization $\langle S_i^\alpha \rangle$ along the ladder in the Υ phase at $\phi = 1.799\pi$ for the 4 degenerate states in the ground state manifold. Results were obtained with DMRG on a cluster of size $N = 154$. The top panel is the ground state (as chosen by DMRG), the rest are the 1st, 2nd, and 3rd (bottom panel) excited states just above the ground state.

off. Importantly, the first 5 points when fitted to a line reveal a non zero intercept of $b = 0.013027$, indicating the presence of some small magnetization for $B = 0$ in the center of the chain. As B is increased, the magnetization in the center grows quite dramatically which agrees with the conclusions from the scaling of the eigenvalues of $\tilde{S}^b$ in the ground state manifold. A true SPT should have a non-magnetic bulk, even in the presence of the magnetic field and hence this phase is probably not an SPT, but rather a short ranged magnetically ordered phase in the plane of the ladder.

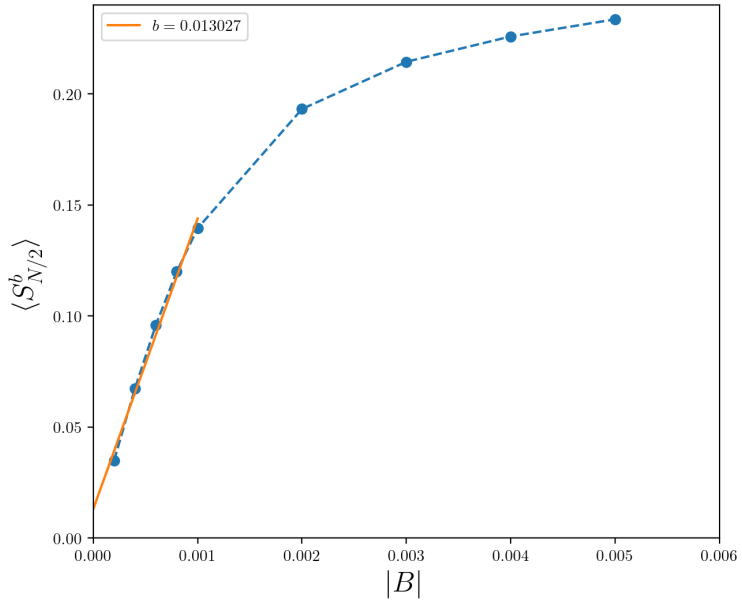

Figure 4.14: Magnetization of the center site $n = N/2$ for $N = 30$ in the Υ phase for $\phi = 1.799\pi$ and $N = 30$. The orange line is a linear fit for the first 5 points that has a non zero intercept b.

4.5.3 The Ω phase

In contrast to the other two phases, the Ω phase does show non trivial edge modes localized only at the edges. The 4 degenerate states in OBC also show some similarity when plotting the on-site magnetization and are difficult to interpret, therefore we apply a small magnetic field to isolate the lowest energy state in the ground state manifold. As the Ω phase has rather large correlation length ($\xi \approx 42.33$), we use $N = 300$ to ensure that the edge modes can be fully separated and a magnetic field $B = -0.0001$. According to Figure 4.5, the only direction which will have a nonzero response to the field is the b axis. The edge modes are clear in Figure 4.15, they vary significantly over one correlation length but then quickly decay into the cluster. Moreover, the response as the edges is much large in magnitude compared to those in the bulk, having near zero values.

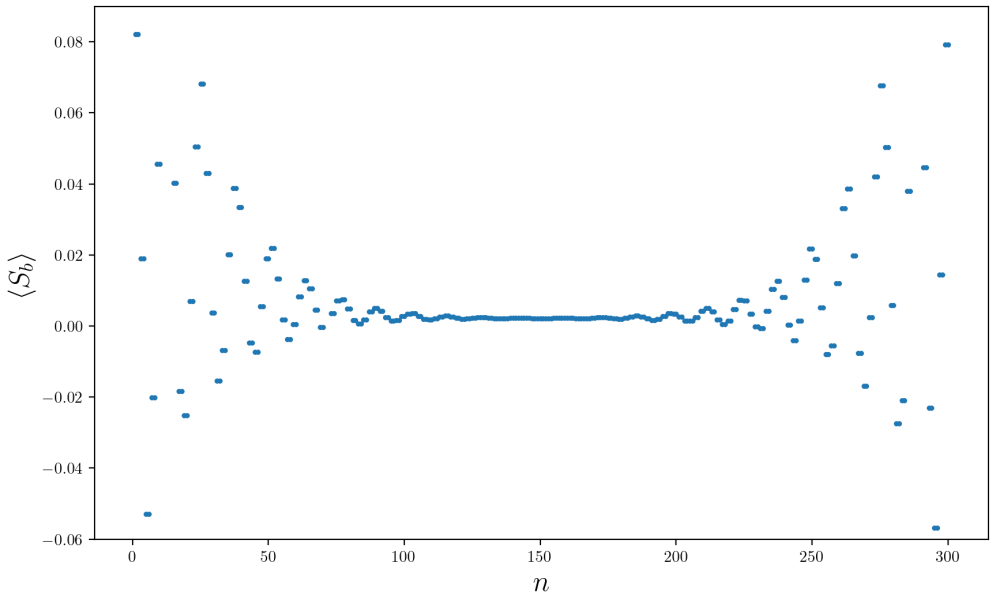

Figure 4.15: Magnetization $\langle S_n^b \rangle$ along the b direction along the length of the ladder with $N = 300$ sites in the Ω phase for $\phi = 1.829\pi$.

Chapter 5

Conclusion

5.1 Summary

In this work we have introduced a minimal theoretical background in one dimensional spin chains. We have introduced the matrix product state formalism of low entanglement states, their efficiency in approximating spin chain ground states in low dimensions, and how they arise as a variational ansatz used by the density matrix renormalization group technique. We also introduced the concept of spin liquids as highly entangled spin states that show no long range magnetic order and that can host non-abelian excitations called anyons. Such systems can be realized in real materials like $\alpha RuCl_3$ where several interactions, like the Γ interaction are present and are argued to be important in understanding these phases. Quasi 2D spin ladder studies simulating these kinds of materials seek to understand their phases, in which particular importance has been placed upon the Γ interaction as its behaviour is not well known.

We then discussed the results of analysing a Hamiltonian with DMRG that contains the Heisenberg and Γ interactions by producing its phase diagram. It yielded 11 phases, 8 that are known or magnetically ordered and 3 potential symmetry protected topological phases, the δ, Υ, and Ω phases. Out of the 3, only the Ω phase seems to be a true SPT while the δ phase is possibly disordered and the Υ phase is magnetically ordered in the honeycomb plane.

5.2 Outlook

The true nature of the δ phase remains to be determined. We have shown that it is a definite phase, with well defined transition points and show clear doubling of the eigenvalues of the reduced density matrix. It is still unclear at this moment if the δ phase is truly gapped as the DMRG data would suggest that it is for finite N, but the gap could decreases for larger values of N as shown by Fig 4.7. Entanglement, energy and correlation length measures seem to indicate that it is a phase, but correlation functions and on site magnetization provide no insight into the phases behaviour. Importantly, the entanglement spectrum shows an exact doubling which is a highly non trivial property to have for a phase related to a simple disordered antiferromagnetic phase to have.

The nature of the Υ and Ω phases are also remaining to be determined. Some more evidence is needed to not only substantiate the claims made in the results section, but to understand the in plane magnetization in the bulk of the Υ phase while explaining the origin of the edge modes in the Ω.

Another avenue would be study the dependence of the ladder on the number of legs the systems has. Here we have only used 2, but in principle this could be increased and can shed some more insight into how the correlation can spread along the rungs where the Γ interaction couple only x, y components of the spin. If the δ phase were to truly be disordered, correlations along the rung direction should also show a lack of magnetic order.

While adding legs is stop gap measure to truly exploring the 2D limit, one could also use iPEPS (infinite projected entangled pair states), a 2d analog of DMRG and MPS that also seek to extract information in the thermodynamic limit. While slower, iPEPS would offer a closer attempt to studying the full honeycomb system, rather than the strip in the ladder.

While previously worked on in other cases [63, 64], a complete projective symmetry analysis of the $J - \Gamma$ model would be useful. This would allow us to determine the number of SPT phases that are allowed in the model, admitted by the full symmetry group of the ladder and the interactions.

Bibliography

[1] J. Bardeen, L. N. Cooper, and J. R. Schrieffer. Theory of superconductivity. *Phys. Rev.*, 108:1175–1204, Dec 1957.

[2] Elliott Lieb, Theodore Schultz, and Daniel Mattis. Two soluble models of an antiferromagnetic chain. *Annals of Physics*, 16(3):407–466, 1961.

[3] F. D. M. Haldane. Nonlinear field theory of large-spin heisenberg antiferromagnets: Semiclassically quantized solitons of the one-dimensional easy-axis néel state. *Phys. Rev. Lett.*, 50:1153–1156, Apr 1983.

[4] Don N. Page. Average entropy of a subsystem. *Physical Review Letters*, 71(9):1291–1294, aug 1993.

[5] J. Eisert, M. Cramer, and M. B. Plenio. Colloquium: Area laws for the entanglement entropy. *Rev. Mod. Phys.*, 82:277–306, Feb 2010.

[6] M B Hastings. An area law for one-dimensional quantum systems. *Journal of Statistical Mechanics: Theory and Experiment*, 2007(08):P08024–P08024, aug 2007.

[7] Itai Arad, Alexei Kitaev, Zeph Landau, and Umesh Vazirani. An area law and sub-exponential algorithm for 1d systems, 2013.

[8] Ming-Chiang Chung and Ingo Peschel. Density-matrix spectra for two-dimensional quantum systems. *Physical Review B*, 62(7):4191–4193, aug 2000.

[9] Ming-Chiang Chung and Ingo Peschel. Density-matrix spectra of solvable fermionic systems. *Physical Review B*, 64(6), jul 2001.

[10] Ingo Peschel, Matthias Kaulke, and Örs Legeza. Density-matrix spectra for integrable models. *Annalen der Physik*, 511(2):153–164, feb 1999.

[11] Kouichi Okunishi, Yasuhiro Hieida, and Yasuhiro Akutsu. Universal asymptotic eigenvalue distribution of density matrices and corner transfer matrices in the thermodynamic limit. *Physical Review E*, 59(6):R6227–R6230, jun 1999.

[12] Ulrich Schollwöck. The density-matrix renormalization group in the age of matrix product states. *Annals of Physics*, 326(1):96–192, jan 2011.

[13] G. Vidal. Classical simulation of infinite-size quantum lattice systems in one spatial dimension. *Physical Review Letters*, 98(7), feb 2007.

[14] C. Eckart and G. Young. The approximation of one matrix by another of lower rank. *Psychometrika*, 1(3):211–218, 1936.

[15] F. Verstraete and J. I. Cirac. Matrix product states represent ground states faithfully. *Physical Review B*, 73(9), mar 2006.

[16] Matthew B. Hastings and Tohru Koma. Spectral gap and exponential decay of correlations. *Communications in Mathematical Physics*, 265(3):781–804, apr 2006.

[17] Chung-Yu Lo, Yoshiki Fukusumi, Masaki Oshikawa, Ying-Jer Kao, and Pochung Chen. Crossover of correlation functions near a quantum impurity in a tomonaga-luttinger liquid. *Physical Review B*, 99(12), mar 2019.

[18] Glen Evenbly and Guifre Vidal. Quantum criticality with the multi-scale entanglement renormalization ansatz, 2013.

[19] G. Evenbly and G. Vidal. Tensor network states and geometry. *Journal of Statistical Physics*, 145(4):891–918, jun 2011.

[20] Ian P McCulloch. From density-matrix renormalization group to matrix product states. *Journal of Statistical Mechanics: Theory and Experiment*, 2007(10):P10014–P10014, oct 2007.

[21] F. Verstraete, J. J. Garcí a-Ripoll, and J. I. Cirac. Matrix product density operators: Simulation of finite-temperature and dissipative systems. *Physical Review Letters*, 93(20), nov 2004.

[22] Steven R. White. Density matrix formulation for quantum renormalization groups. *Phys. Rev. Lett.*, 69:2863–2866, Nov 1992.

[23] E.M. Stoudenmire and Steven R. White. Studying two-dimensional systems with the density matrix renormalization group. *Annual Review of Condensed Matter Physics*, 3(1):111–128, mar 2012.

[24] I. P. McCulloch. Infinite size density matrix renormalization group, revisited, 2008.

[25] Johannes Hauschild and Frank Pollmann. Efficient numerical simulations with tensor networks: Tensor network python (TeNPy). *SciPost Physics Lecture Notes*, oct 2018.

[26] Lev Davidovich Landau. On the theory of phase transitions. I. *Phys. Z. Sowjet.*, 11:26, 1937.

[27] Marcel den Nijs and Koos Rommelse. Preroughening transitions in crystal surfaces and valence-bond phases in quantum spin chains. *Phys. Rev. B*, 40:4709–4734, Sep 1989.

[28] F.D.M. Haldane. Continuum dynamics of the 1-d heisenberg antiferromagnet: Identification with the o(3) nonlinear sigma model. *Physics Letters A*, 93(9):464–468, 1983.

[29] Hal Tasaki. Quantum liquid in antiferromagnetic chains: A stochastic geometric approach to the haldane gap. *Phys. Rev. Lett.*, 66:798–801, Feb 1991.

[30] Wei Chen, Kazuo Hida, and B. C. Sanctuary. Ground-state phase diagram of $s = 1$ XXZ chains with uniaxial single-ion-type anisotropy. *Phys. Rev. B*, 67:104401, Mar 2003.

[31] Sergey Bravyi, Matthew B. Hastings, and Spyridon Michalakis. Topological quantum order: Stability under local perturbations. *Journal of Mathematical Physics*, 51(9), sep 2010.

[32] Xie Chen, Zheng-Cheng Gu, and Xiao-Gang Wen. Local unitary transformation, long-range quantum entanglement, wave function renormalization, and topological order. *Physical Review B*, 82(15), oct 2010.

[33] M. B. Hastings and Xiao-Gang Wen. Quasiadiabatic continuation of quantum states: The stability of topological ground-state degeneracy and emergent gauge invariance. *Phys. Rev. B*, 72:045141, Jul 2005.

[34] C. L. Kane and E. J. Mele. Z_2 topological order and the quantum spin hall effect. *Phys. Rev. Lett.*, 95:146802, Sep 2005.

[35] D. Pé rez-García, M. M. Wolf, M. Sanz, F. Verstraete, and J. I. Cirac. String order and symmetries in quantum spin lattices. *Physical Review Letters*, 100(16), apr 2008.

[36] Xie Chen, Zheng-Cheng Gu, and Xiao-Gang Wen. Classification of gapped symmetric phases in one-dimensional spin systems. *Physical Review B*, 83(3), jan 2011.

[37] Frank Pollmann, Ari M. Turner, Erez Berg, and Masaki Oshikawa. Entanglement spectrum of a topological phase in one dimension. *Physical Review B*, 81(6), feb 2010.

[38] Frank Pollmann and Ari M. Turner. Detection of symmetry-protected topological phases in one dimension. *Physical Review B*, 86(12), sep 2012.

[39] Xie Chen, Zheng-Cheng Gu, and Xiao-Gang Wen. Complete classification of one-dimensional gapped quantum phases in interacting spin systems. *Physical Review B*, 84(23), dec 2011.

[40] Ian Affleck, Tom Kennedy, Elliott H. Lieb, and Hal Tasaki. Rigorous results on valence-bond ground states in antiferromagnets. *Phys. Rev. Lett.*, 59:799–802, Aug 1987.

[41] Alexei Kitaev. Anyons in an exactly solved model and beyond. *Annals of Physics*, 321(1):2–111, jan 2006.

[42] Elliott H. Lieb. Flux phase of the half-filled band. *Physical Review Letters*, 73(16):2158–2161, oct 1994.

[43] A.Yu. Kitaev. Fault-tolerant quantum computation by anyons. *Annals of Physics*, 303(1):2–30, jan 2003.

[44] Lucile Savary and Leon Balents. Quantum spin liquids: a review. *Reports on Progress in Physics*, 80(1):016502, nov 2016.

[45] J. Knolle and R. Moessner. A field guide to spin liquids. *Annual Review of Condensed Matter Physics*, 10(1):451–472, mar 2019.

[46] Chetan Nayak, Steven H. Simon, Ady Stern, Michael Freedman, and Sankar Das Sarma. Non-abelian anyons and topological quantum computation. *Reviews of Modern Physics*, 80(3):1083–1159, sep 2008.

[47] Alexei Kitaev and Chris Laumann. Topological phases and quantum computation, 2009.

[48] G. Jackeli and G. Khaliullin. Mott insulators in the strong spin-orbit coupling limit: From heisenberg to a quantum compass and kitaev models. *Physical Review Letters*, 102(1), jan 2009.

[49] Simon Trebst and Ciarán Hickey. Kitaev materials. *Physics Reports*, 950:1–37, 2022. Kitaev materials.

[50] Giniyat Khaliullin. Orbital order and fluctuations in mott insulators. *Progress of Theoretical Physics Supplement*, 160:155–202, 2005.

[51] Jiř í Chaloupka, George Jackeli, and Giniyat Khaliullin. Kitaev-heisenberg model on a honeycomb lattice: Possible exotic phases in iridium oxides A_2iro$_3$. *Physical Review Letters*, 105(2), jul 2010.

[52] Hong-Chen Jiang, Zheng-Cheng Gu, Xiao-Liang Qi, and Simon Trebst. Possible proximity of the mott insulating iridate Na_2IrO_3 to a topological phase: Phase diagram of the heisenberg-kitaev model in a magnetic field. *Physical Review B*, 83(24), jun 2011.

[53] Robert Schaffer, Subhro Bhattacharjee, and Yong Baek Kim. Quantum phase transition in heisenberg-kitaev model. *Phys. Rev. B*, 86:224417, Dec 2012.

[54] Jiř í Chaloupka, George Jackeli, and Giniyat Khaliullin. Zigzag magnetic order in the iridium oxide na$_2$iro$_3$. *Physical Review Letters*, 110(9), feb 2013.

[55] Jeffrey G. Rau, Eric Kin-Ho Lee, and Hae-Young Kee. Generic spin model for the honeycomb iridates beyond the kitaev limit. *Physical Review Letters*, 112(7), feb 2014.

[56] Jeffrey G. Rau and Hae-Young Kee. Trigonal distortion in the honeycomb iridates: Proximity of zigzag and spiral phases in na2iro3, 2014.

[57] K. W. Plumb, J. P. Clancy, L. J. Sandilands, V. Vijay Shankar, Y. F. Hu, K. S. Burch, Hae-Young Kee, and Young-June Kim. $\alpha - \mathrm{rucl}_3$: A spin-orbit assisted mott insulator on a honeycomb lattice. *Phys. Rev. B*, 90:041112, Jul 2014.

[58] Heung-Sik Kim, Vijay Shankar V., Andrei Catuneanu, and Hae-Young Kee. Kitaev magnetism in honeycomb rucl_3 with intermediate spin-orbit coupling. *Phys. Rev. B*, 91:241110, Jun 2015.

[59] Luke J. Sandilands, Yao Tian, Anjan A. Reijnders, Heung-Sik Kim, K. W. Plumb, Young-June Kim, Hae-Young Kee, and Kenneth S. Burch. Spin-orbit excitations and electronic structure of the putative kitaev magnet $\alpha - \mathrm{rucl}_3$. *Phys. Rev. B*, 93:075144, Feb 2016.

[60] Heung-Sik Kim and Hae-Young Kee. Crystal structure and magnetism in $\alpha - \mathrm{rucl}_3$: An ab initio study. *Phys. Rev. B*, 93:155143, Apr 2016.

[61] A. Banerjee, C. A. Bridges, J.-Q. Yan, A. A. Aczel, L. Li, M. B. Stone, G. E. Granroth, M. D. Lumsden, Y. Yiu, J. Knolle, S. Bhattacharjee, D. L. Kovrizhin, R. Moessner, D. A. Tennant, D. G. Mandrus, and S. E. Nagler. Proximate kitaev quantum spin liquid behaviour in a honeycomb magnet. *Nature Materials*, 15(7):733–740, apr 2016.

[62] Y. Kasahara, T. Ohnishi, Y. Mizukami, O. Tanaka, Sixiao Ma, K. Sugii, N. Kurita, H. Tanaka, J. Nasu, Y. Motome, T. Shibauchi, and Y. Matsuda. Majorana quantization and half-integer thermal quantum hall effect in a kitaev spin liquid. *Nature*, 559(7713):227–231, jul 2018.

[63] Wang Yang, Alberto Nocera, Tarun Tummuru, Hae-Young Kee, and Ian Affleck. Phase diagram of the spin-1/2 kitaev-gamma chain and emergent su(2) symmetry. *Phys. Rev. Lett.*, 124:147205, Apr 2020.

[64] Wang Yang, Alberto Nocera, Erik S. Sørensen, Hae-Young Kee, and Ian Affleck. Classical spin order near the antiferromagnetic kitaev point in the spin-$\frac{1}{2}$ kitaev-gamma chain. *Phys. Rev. B*, 103:054437, Feb 2021.

[65] Erik S. Sørensen, Andrei Catuneanu, Jacob S. Gordon, and Hae-Young Kee. Heart of entanglement: Chiral, nematic, and incommensurate phases in the kitaev-gamma ladder in a field. *Phys. Rev. X*, 11:011013, Jan 2021.

[66] Jacob S. Gordon, Andrei Catuneanu, Erik S. Sørensen, and Hae-Young Kee. Theory of the field-revealed kitaev spin liquid. *Nature Communications*, 10(1), jun 2019.

[67] E. Dagotto, J. Riera, and D. Scalapino. Superconductivity in ladders and coupled planes. *Phys. Rev. B*, 45:5744–5747, Mar 1992.

[68] T. Barnes, E. Dagotto, J. Riera, and E. S. Swanson. Excitation spectrum of heisenberg spin ladders. *Phys. Rev. B*, 47:3196–3203, Feb 1993.

[69] Takafumi Suzuki, Takuto Yamada, and Sei-ichiro Suga. Ground-state phase diagram of anisotropically interacting heisenberg-Γ models on a honeycomb lattice. *Phys. Rev. B*, 103:224425, Jun 2021.

[70] Andrei Catuneanu, Youhei Yamaji, Gideon Wachtel, Yong Baek Kim, and Hae-Young Kee. Path to stable quantum spin liquids in spin-orbit coupled correlated materials. *npj Quantum Materials*, 3(1), apr 2018.

[71] Matthias Gohlke, Gideon Wachtel, Youhei Yamaji, Frank Pollmann, and Yong Baek Kim. Quantum spin liquid signatures in kitaev-like frustrated magnets. *Physical Review B*, 97(7), feb 2018.

[72] Erik S. Sørensen and Hae-Young Kee. Twice hidden string order and competing phases in the spin-1/2 kitaev-gamma ladder, 2023.

[73] Hui Li and F. D. M. Haldane. Entanglement spectrum as a generalization of entanglement entropy: Identification of topological order in non-abelian fractional quantum hall effect states. *Phys. Rev. Lett.*, 101:010504, Jul 2008.

[74] J. Eisert and M. Cramer. Single-copy entanglement in critical quantum spin chains. *Phys. Rev. A*, 72:042112, Oct 2005.

[75] Daniel Gottesman and M B Hastings. Entanglement versus gap for one-dimensional spin systems. *New Journal of Physics*, 12(2):025002, feb 2010.

[76] Zheng-Xin Liu, Min Liu, and Xiao-Gang Wen. Gapped quantum phases for the $s = 1$ spin chain with D_{2h} symmetry. *Phys. Rev. B*, 84:075135, Aug 2011.